ASSESSMENT OF ATMOSPHERIC HEIGHT UNCERTAINTIES FOR HIGH PRECISION SATELLITE ALTIMETER MISSIONS TO MONITOR OCEAN CURRENTS

JULIUS GOLDHIRSH
JOHN R. ROWLAND

SPACE DEPARTMENT
THE JOHNS HOPKINS UNIVERSITY ■ APPLIED PHYSICS LABORATORY

JHU/APL
SIR80U-018
JUNE 1980

ASSESSMENT OF ATMOSPHERIC HEIGHT UNCERTAINTIES FOR HIGH PRECISION SATELLITE ALTIMETER MISSIONS TO MONITOR OCEAN CURRENTS

JULIUS GOLDHIRSH

JOHN R. ROWLAND

The funding for this report was provided by NASA Wallops Flight Center as part of the TOPEX Altimeter Design Study under Purchase Order No. P-78192(G).

SPACE DEPARTMENT
THE JOHNS HOPKINS UNIVERSITY ■ APPLIED PHYSICS LABORATORY
Johns Hopkins Road, Laurel, Maryland 20810
Operating under Contract N00024-78-C-5384 with the Department of the Navy

ASSESSMENT OF ATMOSPHERIC HEIGHT UNCERTAINTIES FOR HIGH PRECISION SATELLITE ALTIMETER MISSIONS TO MONITOR OCEAN CURRENTS

List of Figures

List of Figures (Cont.)

List of Tables

1.0 Introduction

In this report we examine the influence of the atmosphere on nadir directed signals associated with satellite altimeters. Frequencies at 6, 13.5, and 35 GHz are selected so as to provide a parameter study. Uncertainties are summarized in both existing and proposed techniques which establish ionospheric and tropospheric height corrections. The error summary thus gives values describing the "best you can do" in height resolution (as dictated by atmospheric parameters) for a satellite borne altimeter system. The impetus to pursue this effort stems from a possible future satellite experiment for studying ocean surface currents (TOPEX). An altimeter system aboard such a satellite may require mean sea height resolutions significantly better than 10 cm [Nagler and Brown, 1979].

The results presented here reflect data gleaned from the literature, at large, as well as from the existing body of published literature associated with the Seasat A Altimeter Experiment (See References - Section 6.0).

We specifically consider here (1) the effects of precipitation on altimeter signals (Chapter 2) (2), range errors due to refractive index variations in both the clear atmosphere (convective and non-convective) and clouds (Chapter 3), and (3) range errors introduced by the ionosphere (Chapter 4).

The uncertainties introduced by a two frequency altimeter system which continuously corrects range errors introduced by the

ionosphere are examined in Chapter 4. In Chapter 2, a preliminary analysis is pursued establishing the feasibility of incorporating rain rate range gates in a future satellite borne altimeter system.

2.0 Effects of Precipitation on Altimeter Signal

2.1 Range Errors Due to Precipitation

The range error contribution due to a rain medium alone may be expressed as,

$$\Delta R_e \approx \int_0^L \left\{ R_e \, (\tilde{m}-1) \right\} d\ell \qquad (2.1)$$

where $\tilde{m}$ represents the equivalent complex refractive index of a plane-parallel medium containing rain particles as described by Van De Hulst (1957), R_e denotes the real part, $d\ell$ the differential path length, and L the path interval through rain (one way).

The complex part of m gives rise to the attenuation characteristics of the radio waves. In Fig. 1 are given plots of range errors, $\Delta R_e'$ expressed in cm per km path length through rain as a function of rain rate, R (expressed in mm/hr) for 6, 13.5, and 348 GHz. The curve at 34.8 GHz was derived from the phase tabulations of Oguchi (1973) for the horizontal polarization case (distorted raindrops). The curves at 6 and 13.5 GHz were derived from the phase results of Rogers and Olsen (1975), Olsen, et al (1978) and a C.C.I.R. Document 5/23-E (1975) for spherical raindrops. In all case, Laws and Parsons (1943) raindrop size distributions were assumed in the computation of m. It may be noted that similar sets of curves at other frequencies (1.43-300 GHz) may be derived using the equivalent refractive index results of Setzer (1970). In the use of such curves, a note of caution should be included because rain is a dispersive medium. Both the phase and group time delays decrease with increasing frequency, the extent of which depends on the rain. Rogers and Olsen (1975) point out that the theory breaks down at higher frequencies and the results should be used with caution. Examples of the dispersive nature of rain are given in Fig. 2.

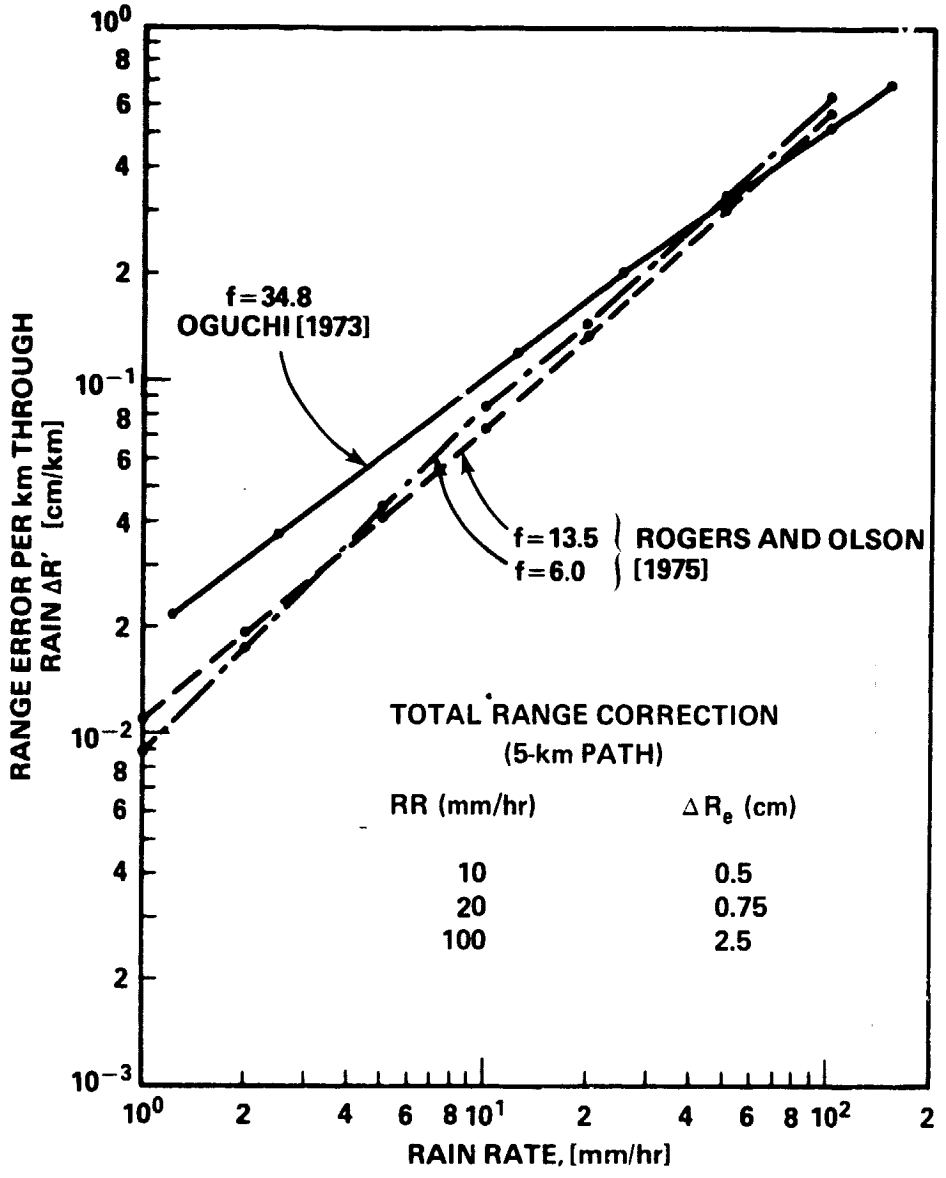

Fig. 1 Range Error per km Through Uniform Rain of Rate R, [mm/hr]

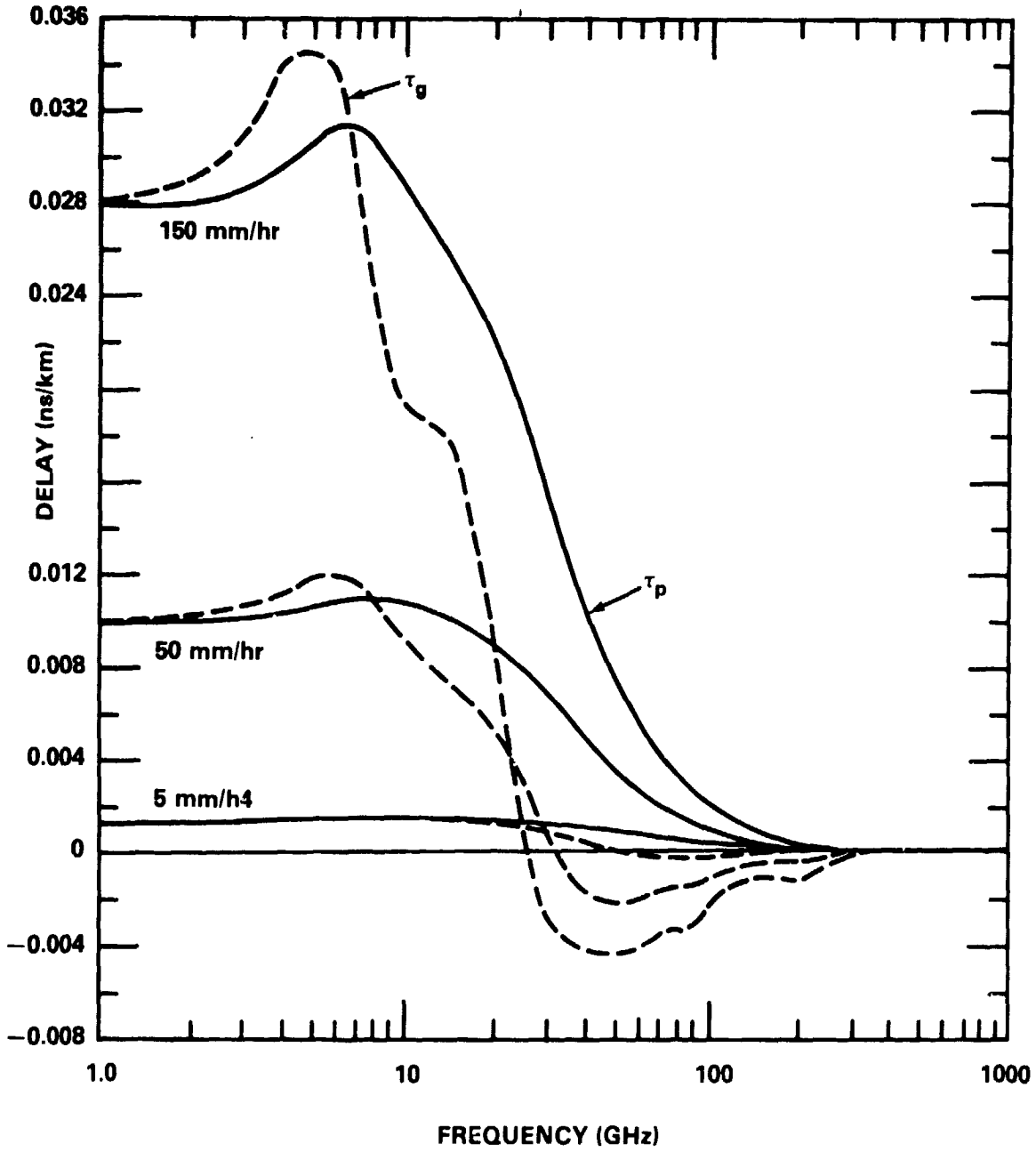

Fig. 2 Time Delay Through Rain vs Frequency [Rogers, 1975]; τ_g and τ_p denote group and phase time delays, respectively.

Although the results depicted in Fig. 1 are derived from the phase refractive indices (as opposed to the group refractive index), they are considered approximately accurate. The differences between the curves of Oguchi and those of Rogers and Olsen in Fig. 1, are due both to computational reasons as well as the fact that Oguchi considers distorted raindrops.

In establishing the overall nadir rain paths, two basic types of rain may be considered; nonconvective (stratiform) and convective (thunderstorm). For stratiform rain types, the rain may be assumed to fall from the $0^{o}C$ isotherm level. Typical heights of the zero degree isotherm for the band of latitudes ranging from $15^{o}N$ to $45^{o}N$ vary from 4.0 to 4.7 km during the month of July (Cole, et al, 1965; Cole and Kantor, 1963). Stratiform type rains are generally widespread (hundreds of km) and have rain rates of less than 20 mm/hr associated with them (C.C.I.R., 1978).

In convective rains, drops are often carried in the supercooled state to several km above the $0^{o}C$ isotherm, and the path interval of rain may be as high as 10 km. This type rain is comprised of isolated intense cells or cells imbedded in rains covering a larger area. The horizontal extent of the intense regions of rain are of the order of several km (C.C.I.R., 1978) and many of such cells may exist within a thunderstorm region. Rain cell dimensions are further characterized in Section 2.4.

We note from the above and the curves in Fig. 1, that for a 5 km nadir rain path and a 100 mm/hr rain (thunderstorm), we obtain a 2.5 cm range error. For a stratiform type rain of 10 mm/hr (moderate rain) over a 5 km path, we obtain a 0.5 cm range error.

Hence, we conclude that the occasional thunderstorm may give rise to a discernible range error whereas the more frequent widespread type rains may be ignored. These conclusions, however, carry with them a few caveats and these are: (1) the more intense rains may give rise to a considerable loss of signal at frequencies above 10 GHz, which may represent a more severe problem than that arising due to range errors (see Section 2.2), (2) widespread rain creates additional brightness temperature which interferes with the ability of auxiliary radiometry measurements to remove the path error due to water vapor in the troposphere (see Section 3.3). For example, the Scanning Multifrequency Microwave Radiometer (SMMR) on Seasat 1 was not always able to accurately retrieve sea surface temperatures in very light rains exceeding 0.5 mm/hr [Seasat Workshop Report, Vol. 1, p. 8-34].

2.2 Attenuation Effects of Precipitation

Raindrops both absorb and scatter radio waves giving rise to attenuation; absorption being the prime contribution at frequencies below 10 GHz. At higher frequencies, scattering becomes important and at around 60 GHz and a rain rate of 5 mm/hr both contributions are approximately equal (Setzer, 1970). At the higher rain rates the scattering contribution may exceed that due to absorption, depending upon the frequency.

In Figure 3 are plotted a set of curves depicting the attenuation coefficients as a function of frequency and rain rates (C.C.I.R., 1978). These curves were obtained from the results of Olsen et al, (1978) assuming a Laws and Parsons (1943) drop size distribution, terminal velocities of Gunn and Kinzer (1949), and the index of refraction of water at 20°C of Ray (1972). We note from Fig. 3 a monotonic increase of attenuation with frequency up to 100 GHz beyond which a leveling off and slight reduction occurs.

In Figure 4 are plotted the attenuation coefficients for the specific frequencies of 6, 13.5, and 35 GHz, as a function of rain rate. These may be expressed by the empirical relations (Olsen et al, 1978),

$$k = aR^b \qquad (2.2)$$

where k = attenuation coefficient (dB/km) at the frequency, f

a, b = empirical frequency and drop size distribution dependent quantitites

R = rain rate (mm/hr)

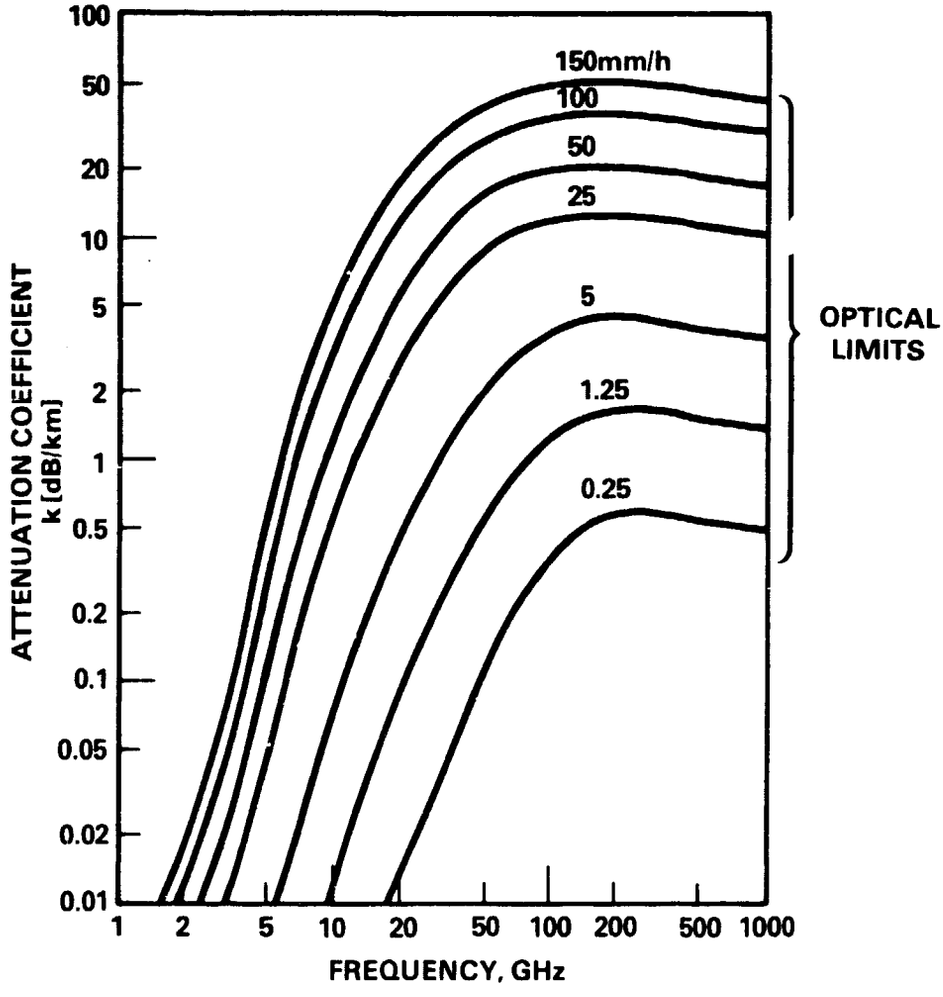

Fig. 3 Attenuation Coefficients as A Function of Frequency at Different Rain Rates [C.C.I.R., 1978]

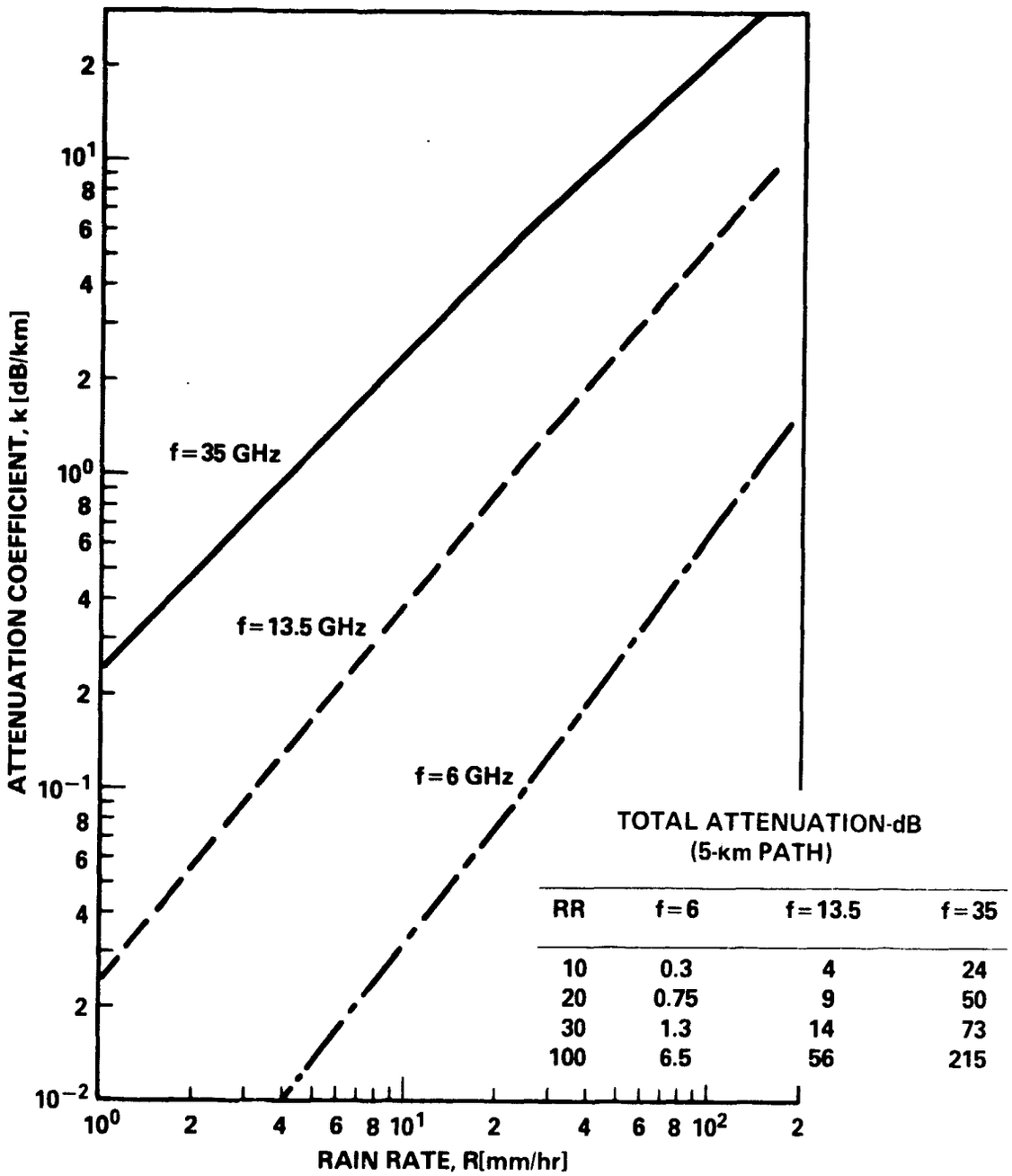

Fig. 4 Attenuation Coefficient as a Function of Rain Rate for Various Frequencies

In Table 1 are given values of a and b at the frequencies given in Figure 4.

Table 1 Values of a and b for $k = aR^b$ Relation [Olsen et al, 1978]

Frequency (GHz)	R < 50 mm/hr		R > 25 mm/hr	
	a	b	a	b
6	1.79×10^{-3}	1.238	1.06×10^{-3}	1.393
13.5	2.48×10^{-2}	1.205	3.46×10^{-2}	1.109
35	2.35×10^{-1}	1.009	3.37×10^{-1}	0.904

We note from Figure 3 that at a 100 mm/hr rain rate, the attenuation coefficients are 0.65, 5.7, and 21.7 dB/km at 6, 13.5 and 35 GHz, respectively. Assuming a 10 km round trip path distance, the total respective attenuations are 6.5, 57 and 217 dB at 100 mm/hr rain rates.

For Seasat A operation (f=13.5 GHz) an approximate 14 dB margin existed before loss of track occurred (at about a signal to noise ratio of 6 dB) whereas optimal operation existed with signal to noise levels above 13 dB. For a two way 10 km path length, 14 dB corresponds to an attenuation coefficient of 1.4 dB/km, which at f = 13.5 GHz, corresponds to a rain rate of about 30 mm/hr (Fig. 4).

The passage through intense rain cells by Seasat A could have resulted in distorted altimeter return signals giving rise to subsequent misinterpretations of wave height. This is evidenced by the sudden appearance of occasional interpreted wave height values up to 15 to 20 m for a distance of thirty kilometers or so (Lorell, 1979). An illustration of a rain cell encounter is depicted in Fig. 5 (Seasat Workshop Report, Vol. 1, p. 5-41). During the encounter we note that scattering cross section, σ^o drops about 1 dB for 4 seconds (28 km along ground track), the significant wave height, $H_{1/3}$ rises from 3 m ambient to a sharp peak of 6 m and drops back to ambient in approximately 1 sec (7 km). The sea surface height is shown to drop about 1 m and return to ambient in about 1 sec.

It is apparent from the attenuation curves in Fig. 4 and the time delay results depicted in Fig. 1, that at the rain rates in which the range errors become a problem for f = 13.5 GHz (and greater frequencies), attenuation becomes prohibitively high, resulting in loss of lock or highly distorted returns. On the other hand, there may be marginal time delays for 6 GHz at the high rain rates (100 mm/hr) where the attenuation is considerably reduced.

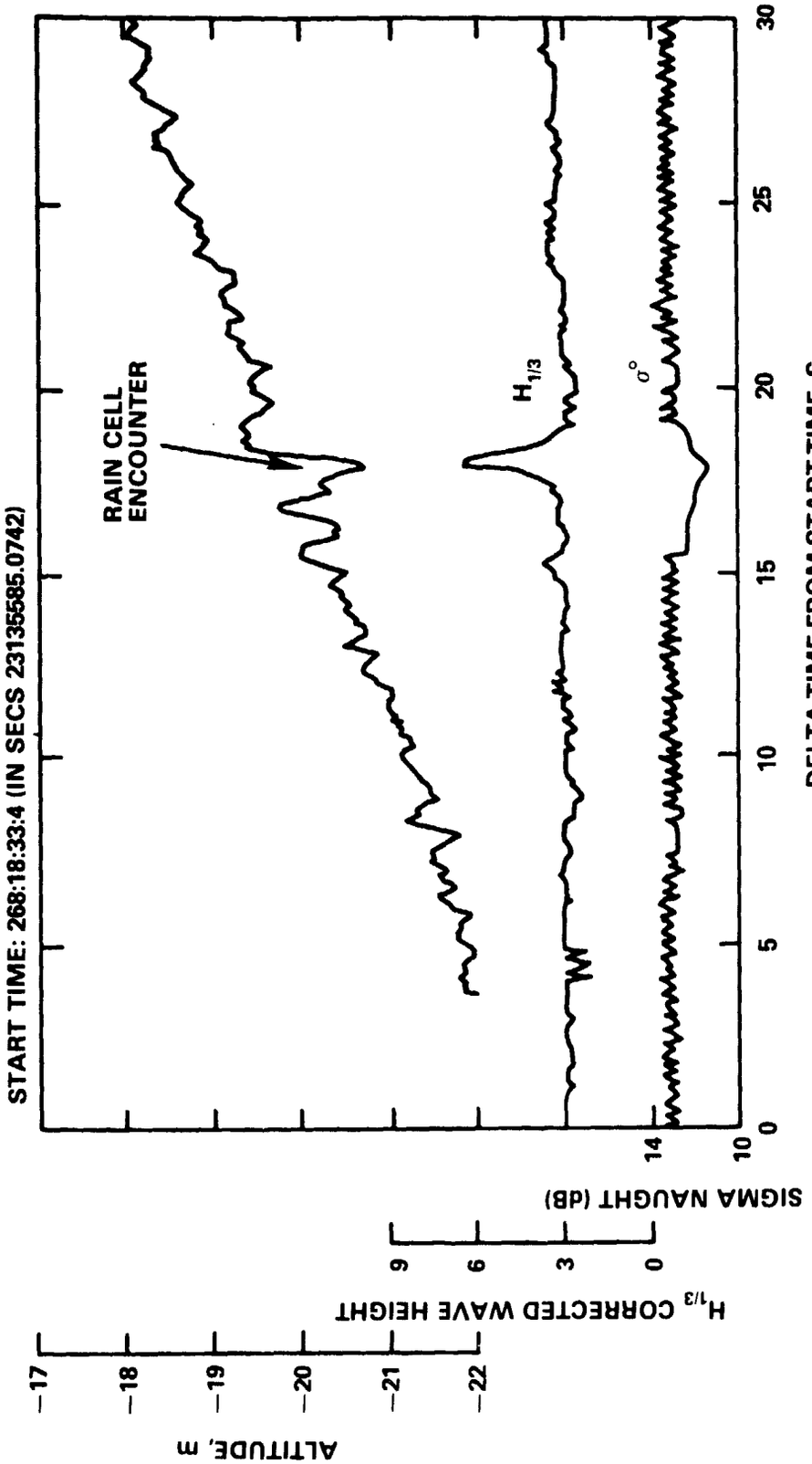

Fig. 5 Response of Seasat Altimeter to a Rain Cell (Seasat Gulf of Alaska Workshop Report, Vol. 1, April 1979)

2.3 Measurement of Earth's Rain Intensity with a Satellite Altimeter

We examine here the power received at the input of a Seasat type altimeter due to rain scattering at frequencies of 6, 13.5, and 35 GHz. The measurement of rain and the corresponding intensity (mm/hr) could serve multifold purposes; namely,

(1) Determination of the existence of rain rate levels could explain deterioration of altimeter performance (e.g., increased noise, and higher uncertainities in mean sea level, significant wave height, and backscatter coefficient of the ocean surface.

(2) Explain poor radiometer performance and establish regions where the atmospheric corrections using radiometry should not be used.

(3) Provide rain rate intensities and vertical profiles on a world-wide scale.

2.3.1 Detectable Power from Rain Scatter for Seasat Type Altimeters

The power scattered from a pulse volume of raindrops is given by (Goldhirsh, 1979)

$$P_r = \frac{c}{1024\pi^2 \ln 2}\left[P_t \tau \lambda^2 G^2 (\Delta\theta_e)(\Delta\theta_h) L_t L_r \frac{\eta}{r^2}\right]$$

$$\times f(B)\ 10^{-0.2\int_0^r (k_g + k_p + k_c)dr} \qquad (2.3)$$

where

c	velocity of light (3 x 10 m/s),
P_t	transmitted power (watts),
τ	pulsewidth (sec),
λ	wavelength (m),
G	antenna gain,
$\Delta\theta_e, \Delta\theta_h$	vertical and horizontal beamwidths (rad),
L_t	transmitted loss factor ($\leq$1.0) (losses from transmitter power measurement point to gain measurement point),
L_r	receiver loss factor ($\leq$1.0) (losses from receiver calibration point to antenna gain measurement point),
η	rain reflectivity (m^{-1}),
r	range (m),
k_g, k_p, k_c	attenuation coefficients due to atmospheric gas, precipitation, and clouds, respectively (dB/km),

The factor f(B) represents the additional loss factor due to the radar receiver frequency response. For a matched filter linear receiver (bandwidth equal approximately to reciprocal of pulsewidth), f(B) has been estimated previously as equal to 0.66 (-1.8 dB) by Nathanson and Smith (1972). More recently, f(B) has been calculated by Doviak and Zrnic (1979), for a Gaussian shape receiver response and rectangular transmitted pulse, and is given by

$$f(B) = \left\{ \coth \frac{\pi B\tau}{2\sqrt{\ln 2}} - \left(\frac{\pi B\tau}{2\sqrt{\ln 2}}\right)^{-1} \right\}. \qquad (2.4)$$

This results in a -2.3 dB loss for the "matched filter" case, where B is the receiver bandwidth (Hz).

At the frequencies considered and for nadir directed rf energy, we may simplify (2.3) by allowing $k_g \approx 0$ and $k_c \approx 0$ (Goldhirsh 1979). We also assume the receiver bandwidth is sufficiently large such that $f(B) \approx 1$. For the case in which Rayleigh theory is applicable (e.g., $f \lesssim 6$ GHz; the raindrop circumference to wavelength ratio $<<1$), Rayleigh scattering theory is applicable and

$$\eta = (\pi^5/\lambda^4)\, |K_o|^2 Z \quad (m^{-1}) \qquad (2.5)$$

where

$$Z = \int_{D_{min}}^{D_{max}} N(D) D^6 \, dD \quad (m^3) \qquad (2.6)$$

The parameter Z is called the reflectivity factor and is defined by (2.6), where N(D)dD is the number of drops whose diameters are between D and D + dD per unit volume (drop size distribution DSD), and D_{max}, D_{min} are the maximum and minimum diameters of the drops sampled in the pulse volume, respectively. The parameters $|K_o|^2$ is dependent on the complex refractive index, and has been tabulated for various frequencies and temperatures by Gunn and East (1954) and Ray (1972). In the frequency range

6 to 35 GHz and for temperatures ranging from 0^{o} to 20^{o}C, $|K_o|^2 \approx 0.9$. At 13.5 GHz Rayleigh theory may not be applicable and a 40% underestimation in reflectivity may result if (2.5) is used (Goldhirsh, 1977). However, within the uncertainties considered here we shall assume (2.5) is valid at both 6 and 13.5 GHz. At f=35 GHz (Goldhirsh, 1977; p. 93)

$$\eta \approx 4.43 \times 10^{-7} Z^{0.745}; \quad f=35 \text{ GHz} \quad (m^{-1}) \tag{2.7}$$

where Z assumes the more convenient units in (2.7) of $(mm)^6/m^3$.

Assuming the altimeter parameters at the three frequencies considered conform to those on Seasat 1; namely,

$$\begin{aligned} P_t &= 2 \text{ kw} \\ \tau &= 3.2 \text{ sec} \\ r &= 800 \text{ km} \\ \Delta\theta_e = \Delta\theta_h &= 1.6^{o} \\ G &= 40.6 \text{ dB} \end{aligned} \tag{2.8}$$

and considering the aforementioned simplications, (2.3) becomes,

$$P_r \text{ (dBm)} = A + B \log_{10} R - 2 aR^b L \tag{2.9}$$

where the Z's in (2.5) and (2.7) have been related to R by,

$$Z = 200 R^{1.6} \tag{2.10}$$

a relationship which has been found to approximately conform to the Laws and Parsons (1943) drop size distribution (approximate stratiform type rain). Also k_p in (3.1) has been related to R via the relation (2.2). That is,

$$k_p = aR^b \tag{2.11}$$

and L in (2.9) is the nadir directed path length (one way) through rain of rain rate, R, assumed uniform in the vertical extent.

In Table 2 are given values of a and b (Olsen et al, 1978) and A and B for 6, 13.5 and 35 GHz used in (2.9).

Table 2 Values of A, B, a and b in the Relationship (2.9)

Frequency (GHz)	A	B	a	b
6	-120	16	1.79×10^{-3}	1.238
13.5	-113	16	2.48×10^{-2}	1.205
35	-101.2	11.9	2.35×10^{-1}	1.009

In Figs. 6 and 7 are plotted the altimeter received power as a function of rain rate as given by (2.9) where in Fig. 6 we compare the 6 and 13.5 GHz cases and in Fig. 7 the 13.5 and 35 GHz cases. The straight lines correspond to the case of negligible attenuation and are asscciated with measurements at the rain tops (i.e., L =0) and the curved lines depict the power received from a pulse volume at the earth's surface where L=5 km.

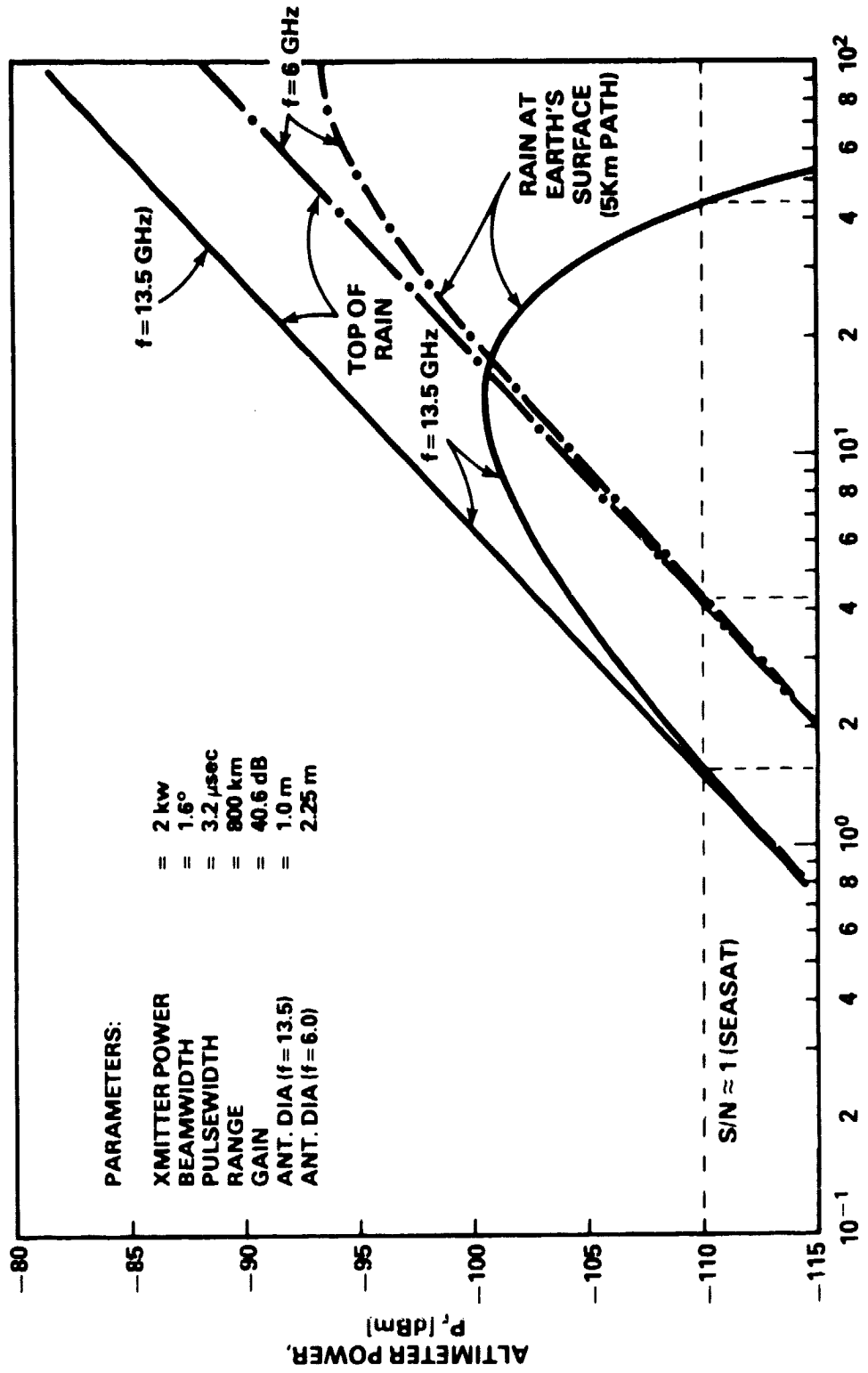

Fig. 6 Power at Receiver Input as a Function of Rain Rate (13.5 GHz vs 6.0 GHz)

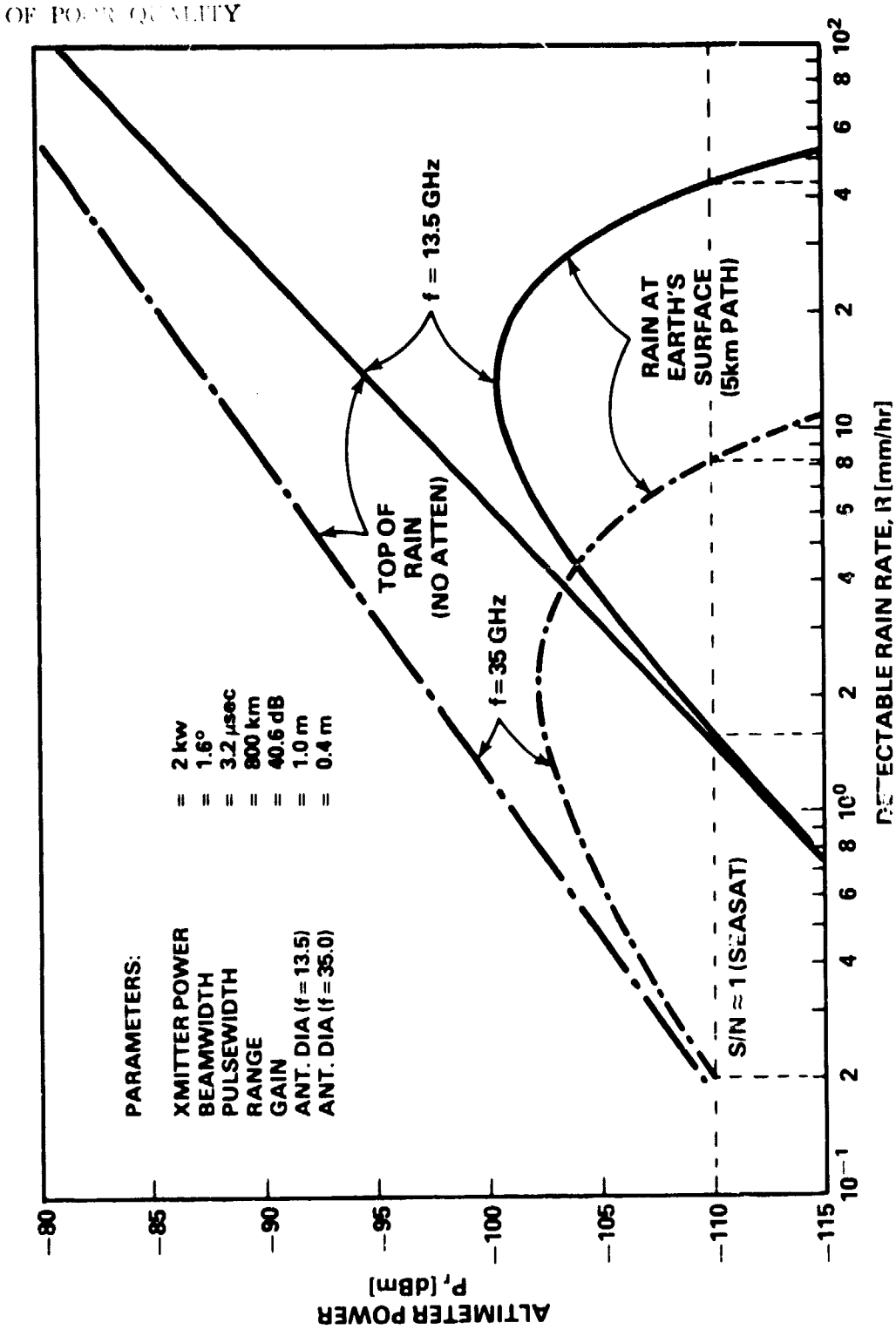

Fig. 7 Power at Receiver Input as a Function of Rain Rate (35 GHz vs 13.5 GHz)

The bending of the power curves in Figs. 6 and 7 are due to two opposing factors in the power relationship as the rain rate increases. At larger rain rates the backscatter reflectivity increases tending to increase the power. However, the path attenuation also increases tending to reduce the power. At rain rates larger than those defined at the curve maxima, the attenuation term dominates over the backscatter reflectivity term and a net reduction in power results.

A nominal value of noise for the satellite altimeter is given by,

$$N = k\ T\ B\ F \longrightarrow -109 \text{ dBm} \qquad (2.12)$$

where

$k = 1.38 \times 10^{-23}$ Joules/^{o}K (Boltzmann's Constant)

$T = 310^{o}$K

$F = 10$ (Noise Figure of Seasat 1)

$B \simeq \frac{1}{\tau} = 3.125 \times 10^{5}$ Hz

We thus note from Figures 6 and 7 that the power scattered from the rain regions may be well above the receiver noise level. For example, a dual wavelength system at 6 and 13.5 GHz would enable the measurement of rain rates above 2 mm/hr (Fig. 6). On the other hand a 35 GHz system would enable rain measurements between 0.2 and 8 mm/hr (Fig. 7).

Improvement of the noise figure in future systems (e.g., F → 5 dB) should result in further enhancement of the signal and enable the determination of a larger range of rain rates.

2.4 Rain Cell Dimensions

Considerable ambiguity exists as to the diameter of rain regions. Many investigators have characterized cell dimensions (C.C.I.R., 1978), however these values are very much dependent on the definition. In actuality, both stratiform type and thunderstorm rains often contain many embedded regions of intense rainfall. Hence, peaks and valleys of rainfall intensity often exist along the horizontal direction, which makes it difficult to relate a rainrate to a rainfall dimension. Notwithstanding this type of ambiguity, we depict two rainfall models in Fig. 8 (taken from Skolnik, 1974) giving the storm diameter as a function of rain rate; namely that of Edgar et al (1973) and Nathanson (1969). We note that 20 km rainfall diameters and larger coexist with rainfalls of 10 to 15 mm/hr and less. (This compares with a footprint of 22 km for a 1.6^{o} beamwidth at 800 km range.) Rainfalls having larger rainrates are confined within smaller diameters and may not fill the pulse volume. A reduced value of scattered power may result for such cases due to averaging within the pulse volume.

Median values of rainfall rates as a function of height have been described by Goldhirsh and Katz (1979) based on a large sampling of radar measurements (Konrad; 1978). These median values, which are plotted as a function of ground category level of reflectivity factor in Fig. 9, show that within $\pm$ 2.5 dBz (dBz = 10 Log_{10} Z [$\mathrm{mm}^6/\mathrm{m}^3$]), the rainfall rates are relatively uniform up to approximately the zero degree isotherm, above which they fall off rapidly. The fall-off of reflectivity occurs at the higher altitudes with increased ground values of Z probably due to convective updrafts carrying the precipitation to higher altitudes.

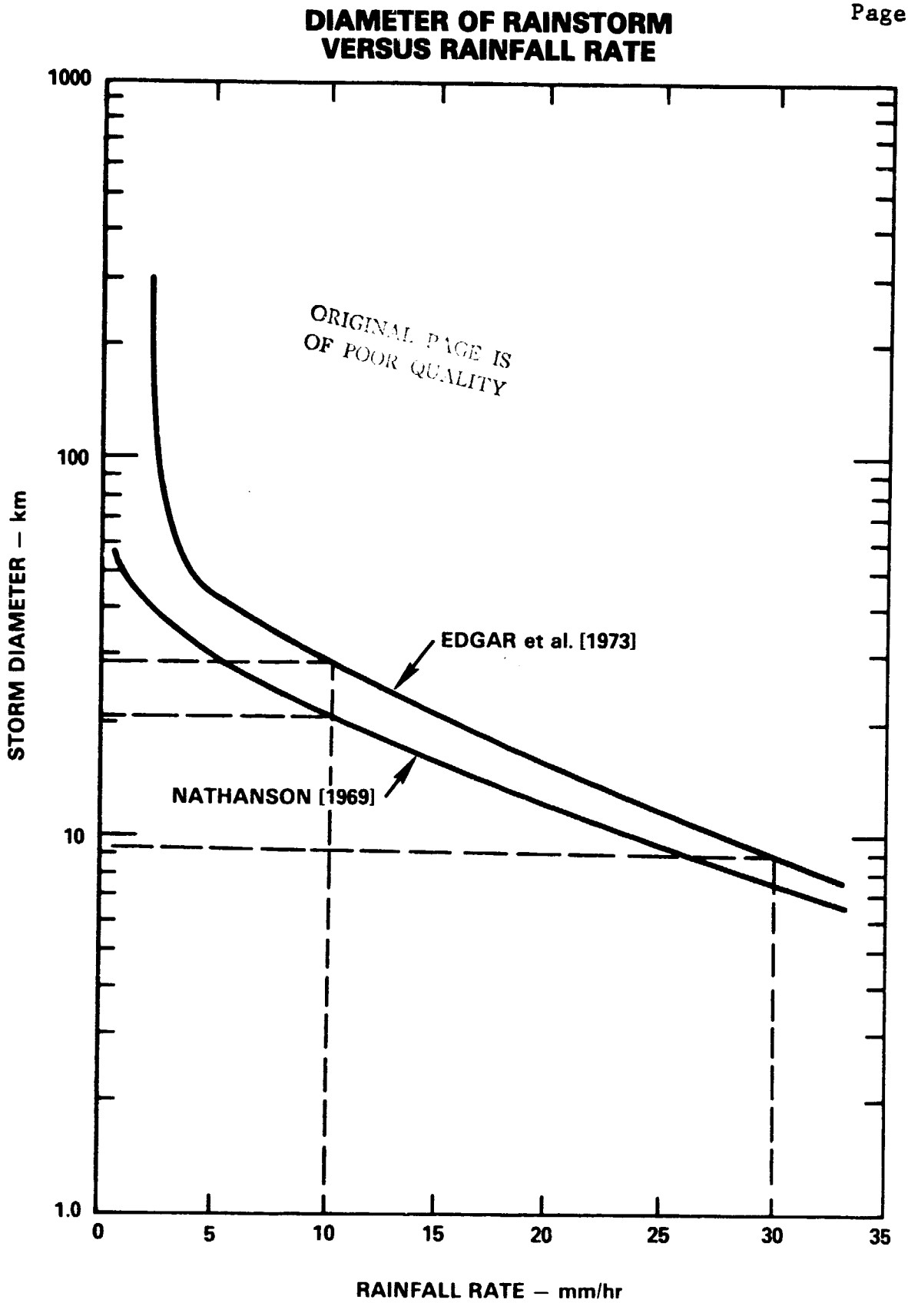

Fig. 8 Diameter of Rainstorm Vs Rainfall Rate

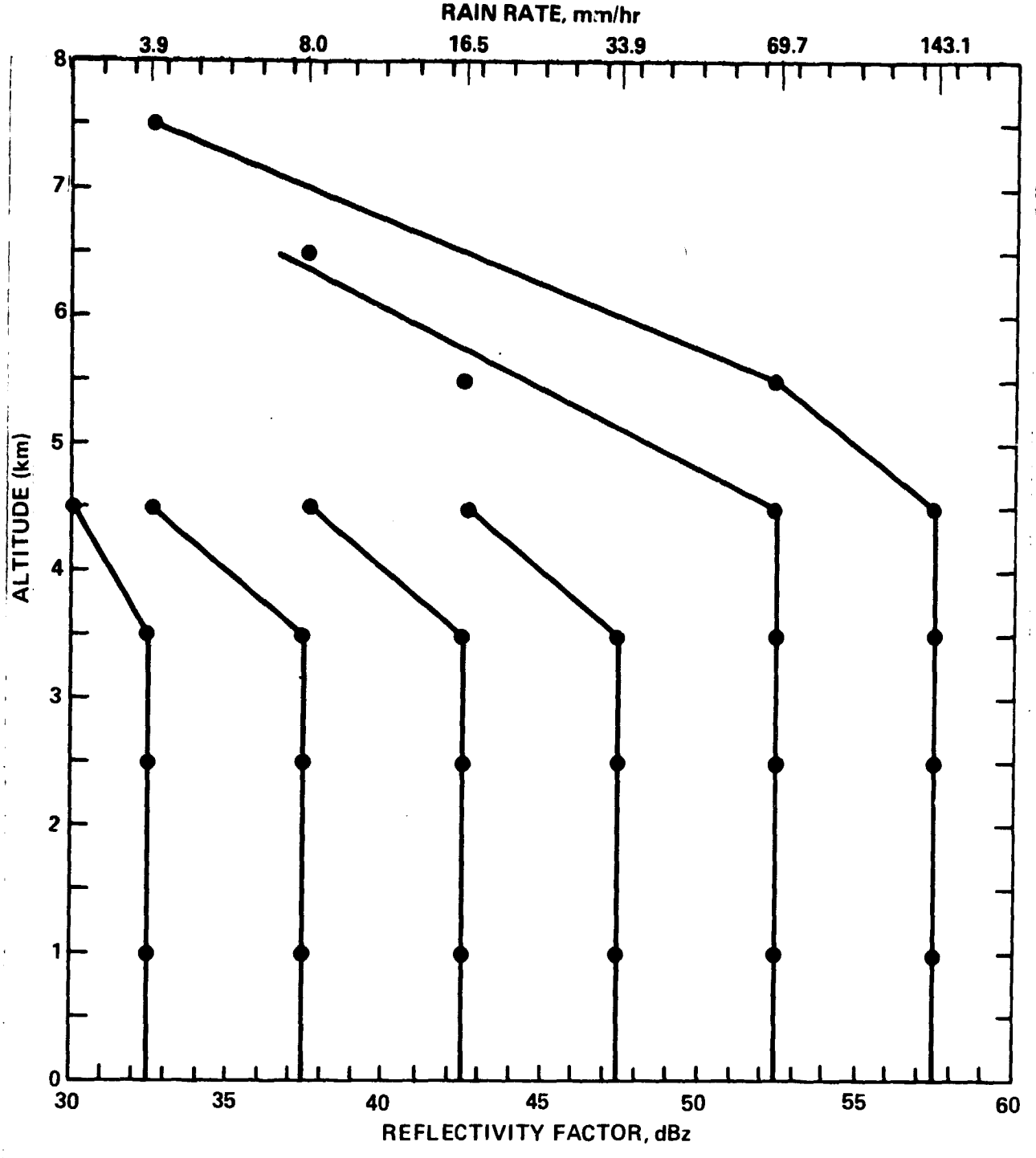

Fig. 9 Median Reflectivity Factor Profiles for Given Ground Categories as Measured at Wallops Island, Virginia [Goldhirsh and Katz; 1979]

3.0 Height Corrections Due to Refractive Index Variations in the Troposphere

3.1 Clear Air Regions - Formulation

The height correction associated with propagation through the troposphere at nadir is given by,

$$\Delta H = \int_{o}^{H} (n-1)\, dh \tag{3.1}$$

where n = the refractive index. It is convenient to define the refractivity, N, as given by

$$N = 10^6\ (n-1) \tag{3.2}$$

where N may be approximated by [Smith and Weintraub, 1953]

$$N = 77.6\ \frac{P}{T} + 3.73 \times 10^5\ \frac{e}{T^2} \tag{3.3}$$

where,

P = total atmospheric pressure [mbar]

e = partial pressure of water vapor [mbar]

T = atmospheric temperature [^{o}K]

The constants in (3.3) are considered valid to 0.5% in N for frequencies up to 30 GHz and normally encountered ranges of pressure, temperature, and humidity and with the exception of the oxygen constituent up to 72 GHz [Bean and Dutton, 1968]. Substitution of (3.3) into (3.1) results in,

$$\Delta H = 77.6 \int_0^H \frac{P}{T}\, dh + 3.73 \times 10^5 \int_0^H \frac{e}{T^2}\, dh \qquad (3.4)$$

or

$$\Delta H = (\Delta H)_{DRY} + (\Delta H)_{WET} \qquad (3.5)$$

where the dry and wet parts refer to the integral expressions of the first and second terms in (3.4).

3.2 Dry and Wet Terms as a Function of Surface Parameters

The height correction as given by (3.4) requires a knowledge of P, T, and e along the propagation path. Although those quantities may be obtained using radiosonde data, they are, in general, unknown, and simplifications of the dry and wet parts of (3.4) in terms of the surface parameters are desirable. The Seasat experimenters [Seasat Users Handbook, 1979] employed the Saastamoinem model [1972], given by,

$$(\Delta H)_{WET} = 2.277 \times 10^{-3} [.05 + \frac{1255}{T_s}]\, e_s \quad [m] \qquad (3.6)$$

$$(\Delta H)_{DRY} = [2.277 \times 10^{-3} - 1.11 \times 10^{-5} \cos\phi] P_s \ [m] \qquad (3.7)$$

where the subscript s denotes the surface parameters and ϕ is the latitude (T_s is in units of ^oK and e_s and P_s are in mbar).

In the determination of the wet term, (3.6), the following assumptions are made:

(1) The temperature reduces with altitude at a constant lapse rate given by,

$$T = T_s + \beta\ (h - h_s) \tag{3.8}$$

where $\frac{dT}{dh}$ = constant temperature lapse rate

h_s = surface altitude above sea level.

(2) The partial pressure of water vapor varies with altitude according to the relation,

$$e = e_s \left(\frac{T}{T_s}\right)^{-k} \tag{3.9}$$

where $k = \frac{4g}{R\beta}$ (3.10)

where g = gravity constant

R = gas constant of dry air

In the absence of SMMR data, Seasat experimenters used interpolated surface values obtained primarily from the Fleet Numerical Weather Center (FNWC).

3.3 Seasat Scanning Multi-Frequency Microwave Radiometer [SMMR] Measurements of the Wet Term

The Seasat radiometer system operated at frequencies of 6.6, 10.7, 18, 21 and 37 GHz at vertical and horizontal

polarizations. Using these measurements the integrated columnar water vapor mass density, W [gm/cm^2] may be measured. That is,

$$W = \int_0^H \rho_v dh \qquad [gm/cm^2] \tag{3.4}$$

where ρ_v is the water vapor density in gm/cm^3.

Assuming the ideal gas law, an atmosphere of constant density, and a temperature profile with a constant lapse rate, the wet height correction term has been shown to be given by [Lipes, 1979; Seasat User's Handbook, 1979],

$$\Delta H_{WET} = W \left[k_2 \left(\frac{R}{M}\right) - k_3 \left(\frac{R}{M}\right)\left(\frac{1}{T_D}\right) \ln \left(1 - \frac{T_D}{T_s}\right)\right] \tag{3.12}$$

where

- W = the SMMR measured integrated water vapor density
- R = ideal gas constant
- M = molecular weight of water
- T_s = surface temperature (air)
- T_D = temperature difference between the surface and the scale height
- k_2, k_3 = constants related to the wet terms of the refractive index

3.4 Comparisons of Seasat Range Corrections with those from Radiosonde Data

In order to arrive at measures of uncertainties for the altimeter height corrections, we compare here actual measurements taken during Seasat operation with those obtained using radiosonde data. For one set of data we examine four passes over Bermuda (passes 1117, 1160, 1246, 1375) and for the second set, we examine the results of four additional passes (1163, 1212, 1292, 1298) taken aboard the Oceanographer Vessel near the Gulf of Alaska taken as part of the GOASEX (Gulf Of Alaska Surface EXperiment). The original data examined here were extracted from the Seasat Gulf of Alaska Workshop Report, Vol. 1, April 1979. Radiosondes were taken during the eight passes to provide "truth measurements".

Two algorithms were used for converting the SMMR data to altimeter path length corrections and these are known as the Wilheit and the Wentz algorithms. In Fig. 10, we compare the results of Wentz and Wilheit with those obtained using radiosonde data for the 8 passes mentioned above [Seasat Gulf of Alaska Workshop Report;1979] . Those radiosonde points labeled "est" correspond to cases in which the measured profiles terminated prematurely and estimated corrections were employed.

In Tables 3 and 4 we summarize the results for the Bermuda passes (Table 3) and the combined Bermuda-Gulf of Alaska passes (Table 4).

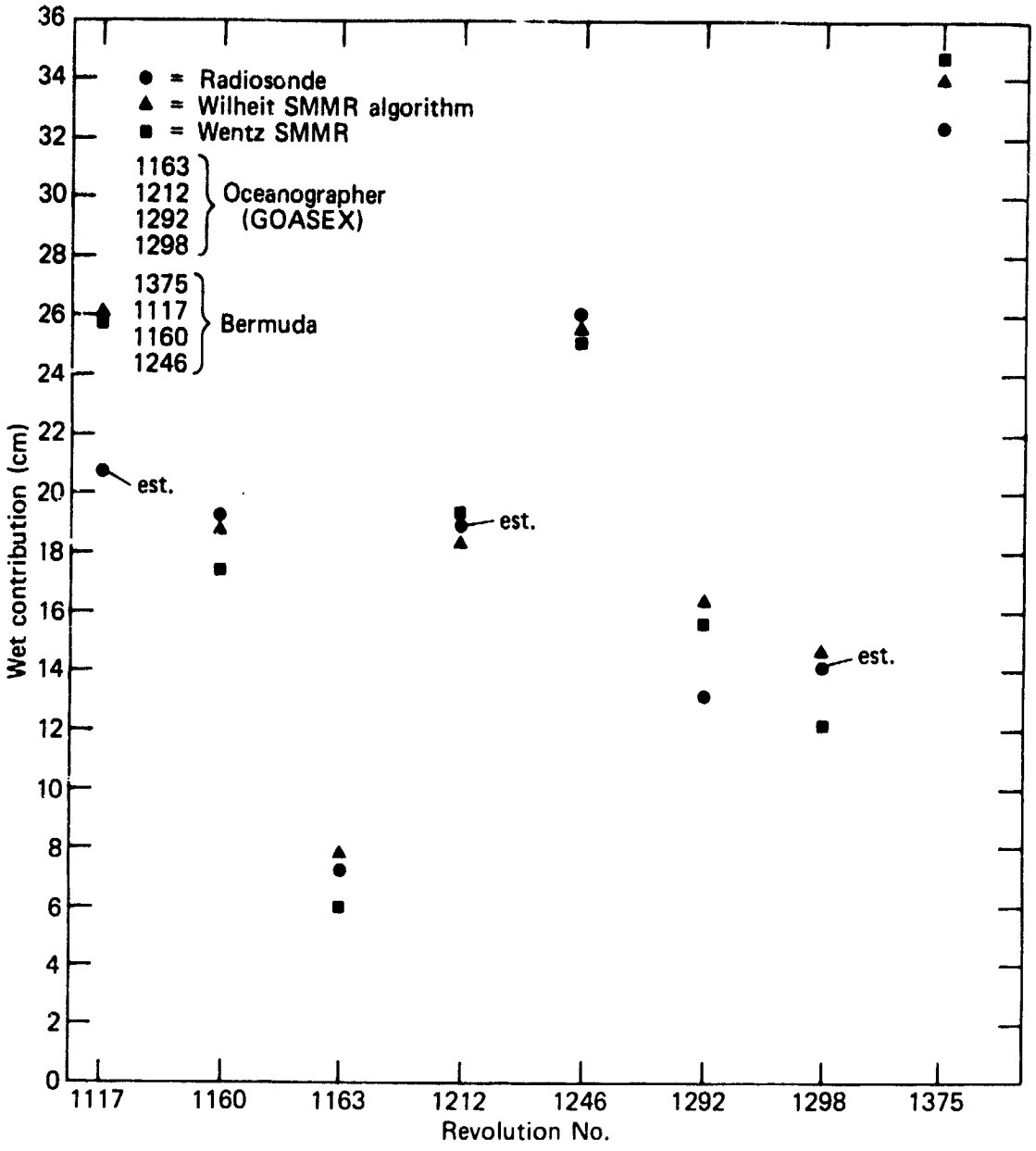

Fig. 10 Comparison Between Altimeter Path Length Correction Algorithms and Radiosonde Data (Seasat Gulf of Alaska Workshop Report; 1979)

Table 3

COMPARISON OF RADIOSONDE WITH MODEL AND SMMR HEIGHT CORRECTIONS

(Seasat A Calibration Passes, 9/13, 9/16, 9/22, 10/1; 1978)
(Seasat Gulf of Alaska Workshop Report, Vol. 1, April 1979)

TYPE	rms Dif.		MAX. Dif.	
	CM	%	CM	%
SMMR	2.5	12.5	5	24
INSITU(P,T,e)	3.5	13.5	5	15
Theor. Model				
FNWC (P,T,e)	5.5	24	7	33
DRY TERM INSITU VS FNWC	1.5	0.7	2	0.9

NOTE:

1) Average Correction for Wet Term (Radiosonde) = 24.75 cm

Table 4

COMPARISON OF SMMR AND RADIOSONDE HEIGHT CORRECTIONS

(8 RADIOSONDE PASSES)
(Seasat Gulf of Alaska Workshop Report, Vol. 1, April 1979)

SMMR ALGORITHM TYPE	rms Dif.		MAX. Dif.	
	CM	%	CM	%
Wilheit	2.3	13	5.5	26
Wentz	2.4	14	5.0	24

The first two columns of Table 3 represent the rms and % rms differences and the last two columns the maximum and % maximum differences. In the first three rows the differences are taken relative to the radiosonde truth corrections, and in the last row the theoretical models for the dry term are compared using the FNWC and surface measurements; the latter representing the assumed "truth" values. In comparing the SMMR measurements, the average values deduced from the Wentz and Wilheit algorithms were used. In Table 4 the uncertainties in the Wentz and Wilheit algorithms are individually compared with the 8 radiosonde passes.

In Fig. 11 the height corrections using the Wentz and Wilheit algorithms are compared with each other and with the theoretical model using FNWC estimates for Revolution 1375. It is interesting to note that a 2 cm rms difference exists when the Wilheit correction is compared to the reference Wentz case (as an example) and an approximate 6 cm rms difference exists upon comparing the theoretical model using FNWC surface estimates with the average of the Wentz and Wilheit cases.

Based upon the results in Tables 3 and 4 and Fig. 11, we conclude that the radiometer measurements give rise to a nominal rms height correction uncertainty of 2.5 cm and the theoretical models uncertainties for the wet and dry terms using FNWC interpolated surface values are approximately 6 cm and 2 cm, respectively.

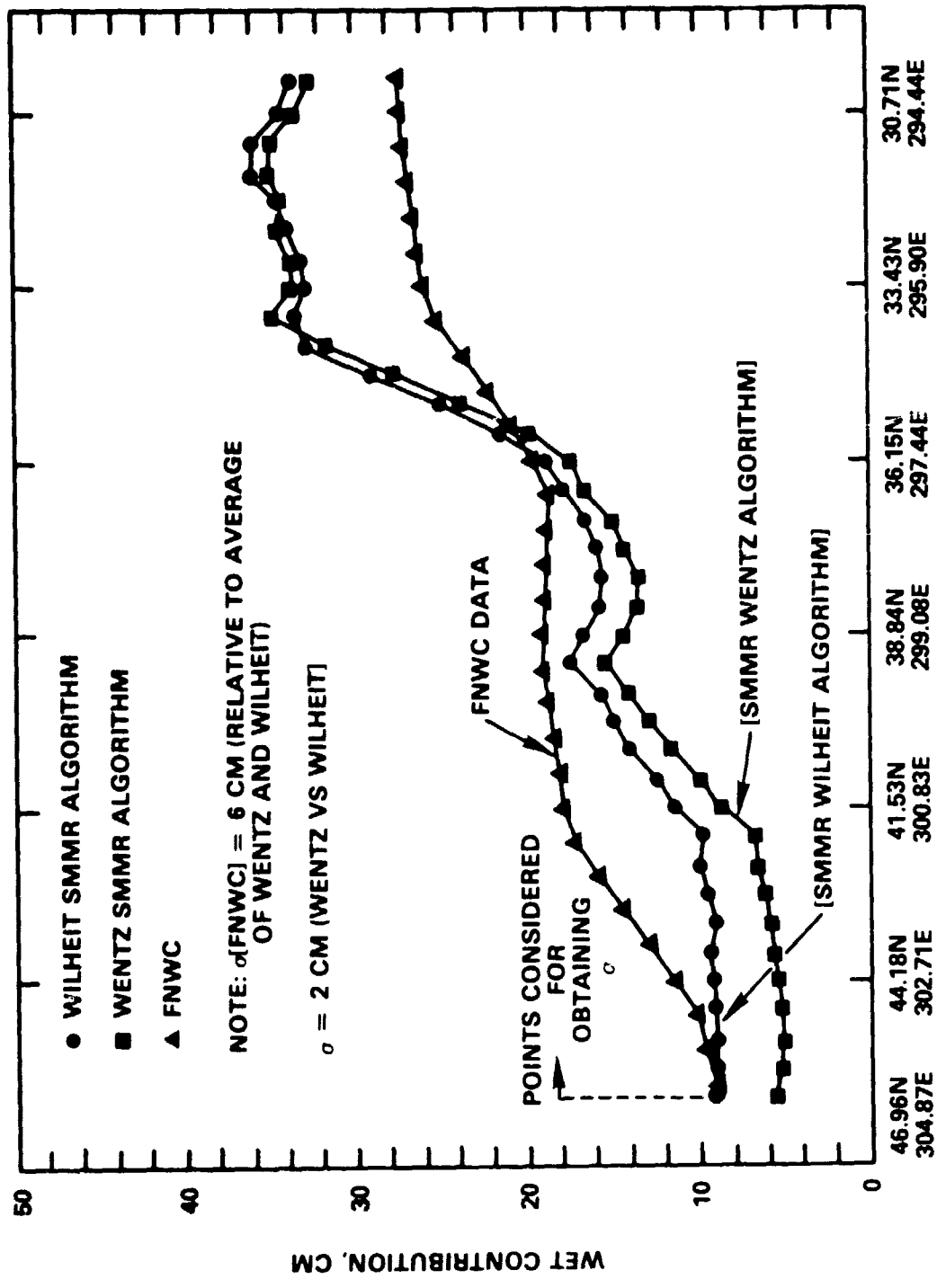

Fig. 11 Comparison of SMMR Algorithms and Tropospheric Correction Model (FNWC Data) - (Seasat Gulf of Alaska Workshop Report;1979).

3.5 Height Correction Fluctuations in the Clear Atmosphere and Due to Clouds

Clouds

In Figs. 12 and 13 we show two cases of refractive index variations through clouds [Campen et al. 1961] obtained with a refractometer located aboard an aircraft. The indicated refractive index values represent the averages of approximately 30 passes through the clouds at the various indicated heights for Boston, Mass. (Fig. 12) and Tucson, Arizona (Fig. 13). In the former case, the cloud extends from approximately 1.8 to 3.5 km and has a maximum horizontal dimension exceeding 1 km. Relative to regions outside the cloud, refractive index changes as high as 25 N units appear over a 1 km horizontal extent. For the case of Fig. 12, integrating N as a function of altitude results in a localized height of 2.3 cm.

The cloud in Fig. 13 extends from 3.8 to 5.8 km with a maximum horizontal extent of approximately 2.5 km and a maximum N (relative to the outside of cloud) of 10. Integration of N over the altitude extent of the cloud for this case results in a 1.8 cm fluctuation of the height.

We thus note that cumulus type clouds may, in fact, result in fluctuations of ΔH of a few cm. It is interesting to note that bands of such clouds may develop in the form of cloud

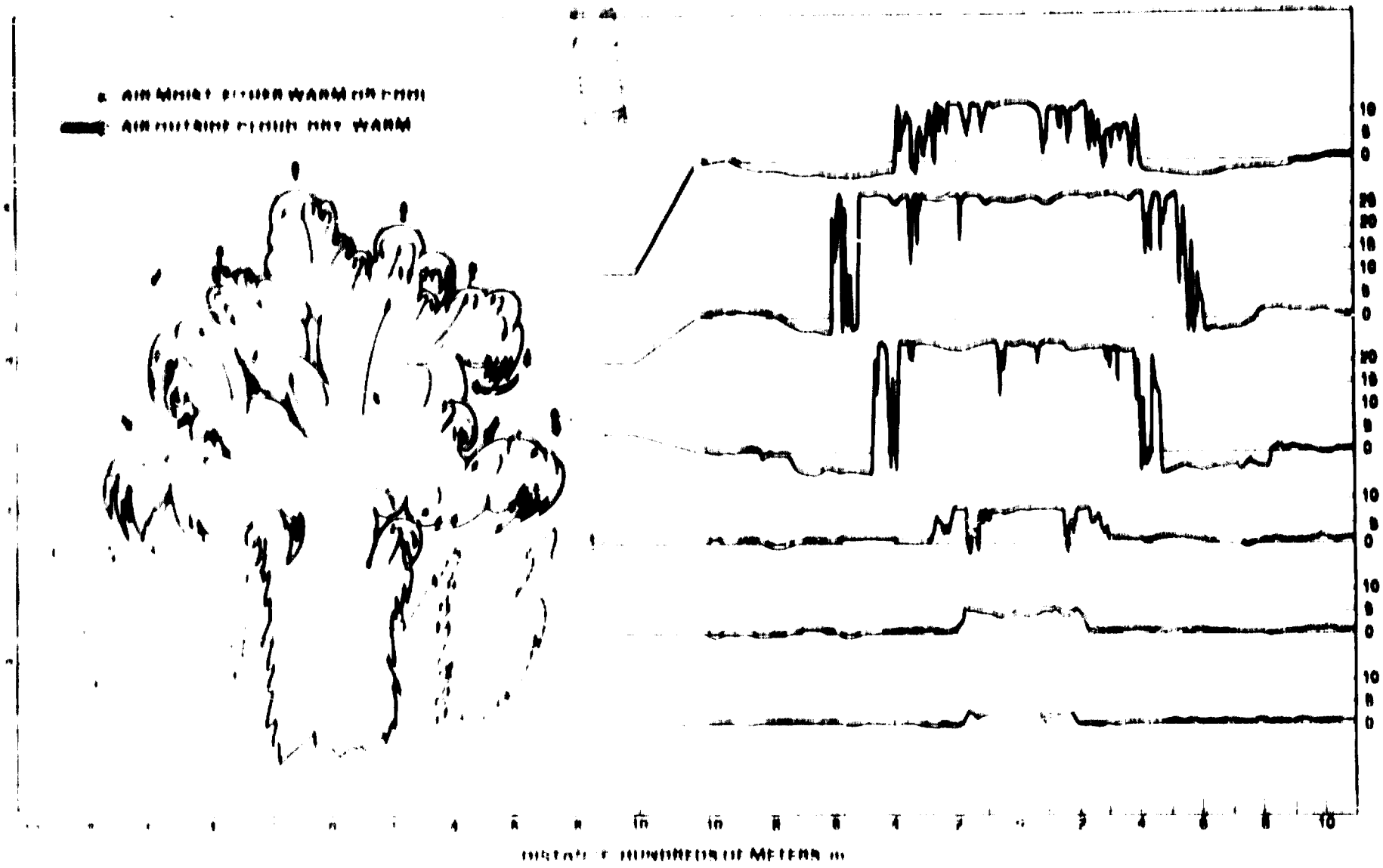

Fig. 12 Average Refractive Index Fluctuations in Cloud for Boston (June 30, 1953) - 30 Cloud Passes - (Campen et al, 1961)

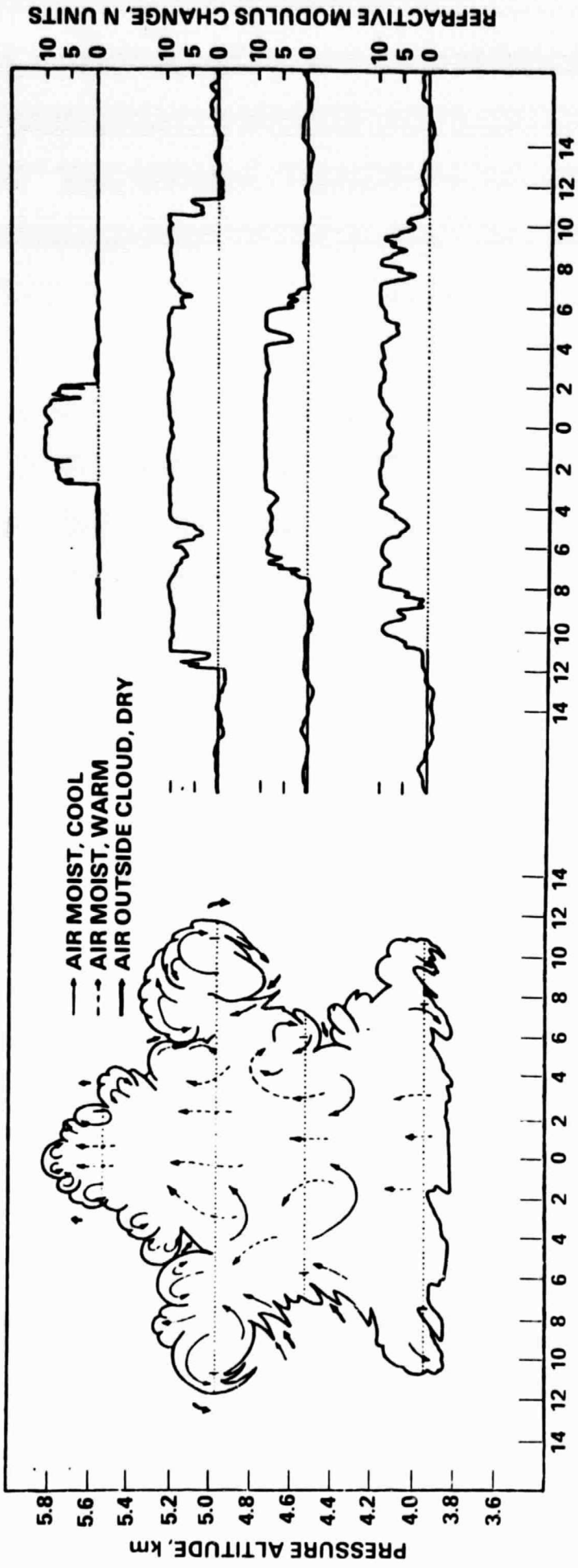

Fig. 13 Average Refractive Index Fluctuations in Cloud for Tucson, Arizona (July 19, 1955) - [Campen et al, 1961]

streets as depicted in Fig. 14 which is a photo as seen from Appolo 6 [Kuettner, 1971]. The length of the streets may extend over 100 km with a spacing of 2 to 2.5 km.

Clear Air Convective Regions

Similar type variations in refractive index may occur in the clear air at the boundaries of moist and dry air. An example of aircraft measurements of the refractive index variations at Wallops Island, Virginia is given in Fig. 15 [Konrad, 1970a]. Intensity modulated displays (RHI's - vertical scans, and PPI's - azimuthal scans) of clear air convective cells taken at Wallops Island, Virginia, are given in Fig. 16 and 17 [Konrad, 1970b]. From figures of these type, it may be demonstrated that ΔH variations and spatial structures are similar to those for cumulus clouds. A typical model for Wallops Island, Virginia of the ΔN variation for a convective field is given in Fig. 18.

In Table 5 is given a summary of the scale dimensions for cloud and clear air convective regions. If the footprint of an altimeter is within the scale dimensions indicated here, rapid fluctuations of the height correction of a few cm may result; other wise smoothing occurs.

Fig. 14 Cloudstreets over Georgia Developing Near the Coastline in a Southerly Flow on April 4, 1968, as seen from APPOLO 6, Maximum Length of Bands; over 100 km, Spacing 2 to 2.5 km [Kuettner, 1971]

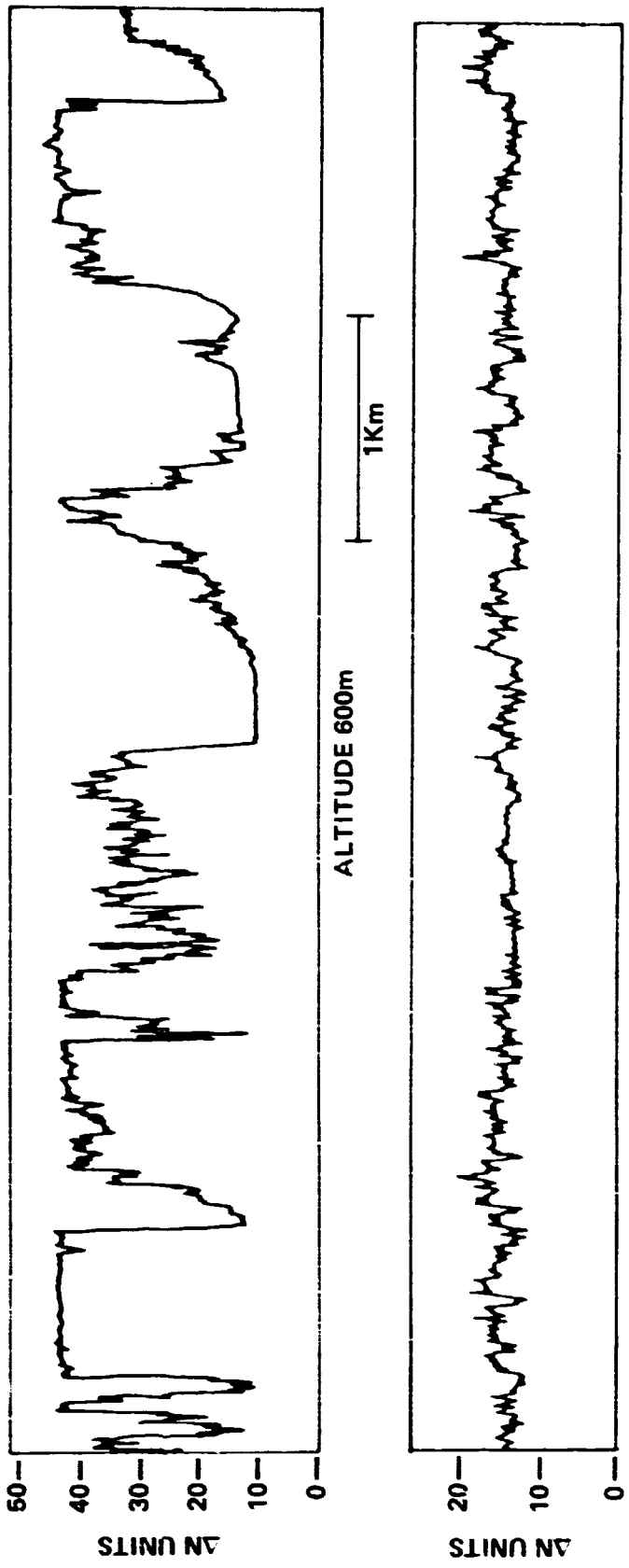

Fig. 15 Aircraft Measurements in Clear Air Convection in Wallops Island, Virginia [Konrad, 1970a]

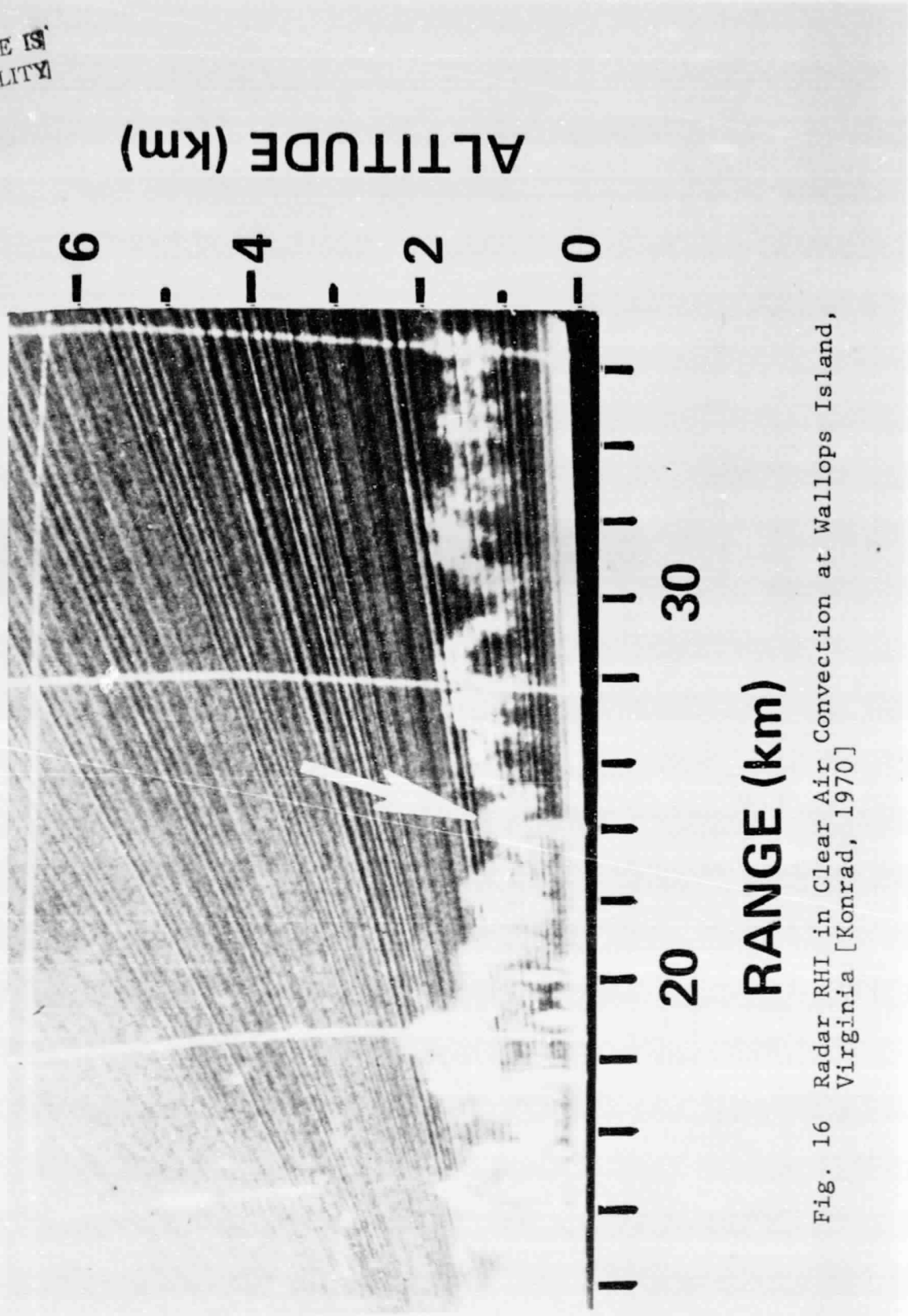

Fig. 16 Radar RHI in Clear Air Convection at Wallops Island, Virginia [Konrad, 1970]

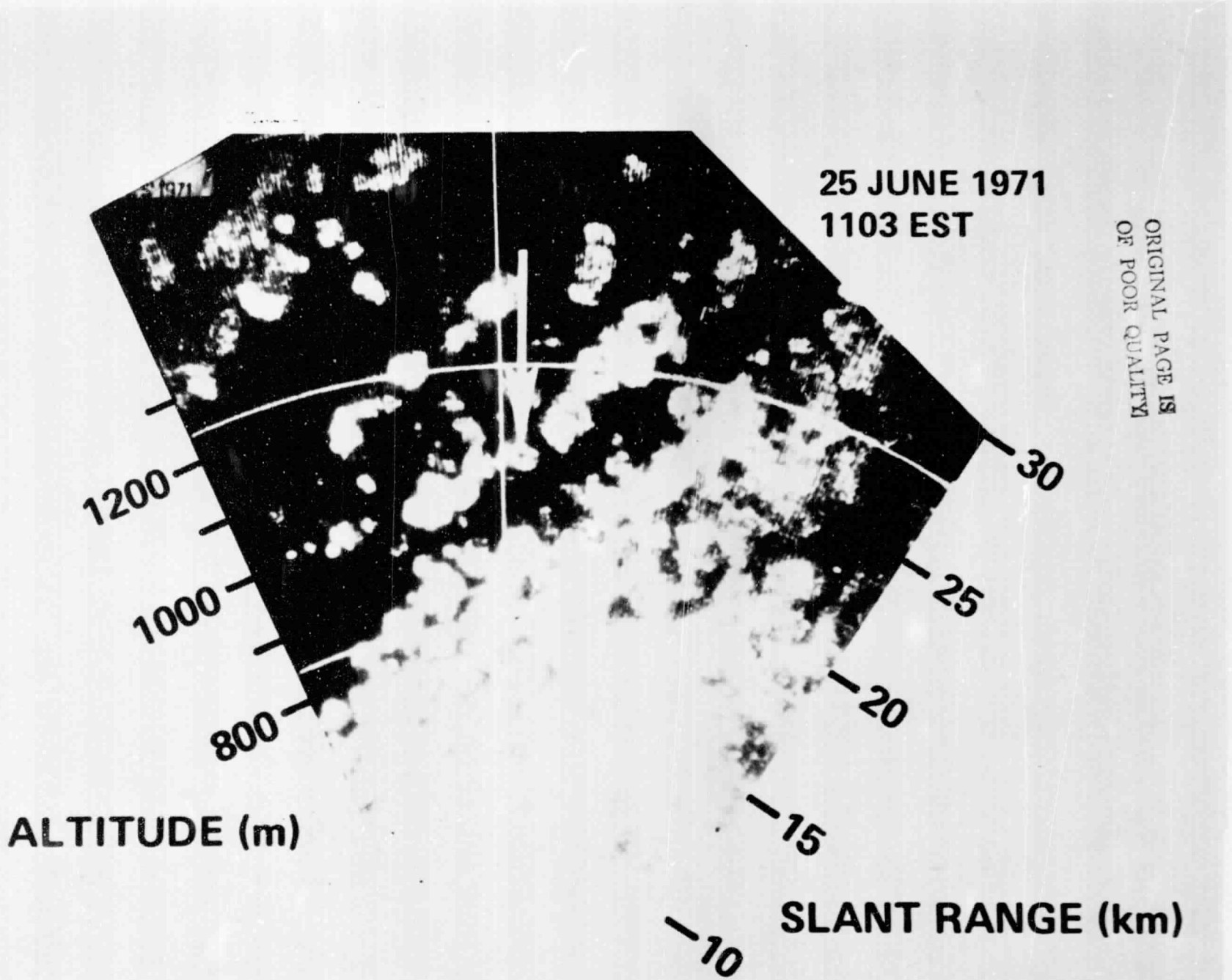

Fig. 17 Radar PPI in Clear Air Convection at Wallops Island, Virginia [Konrad, 1970]

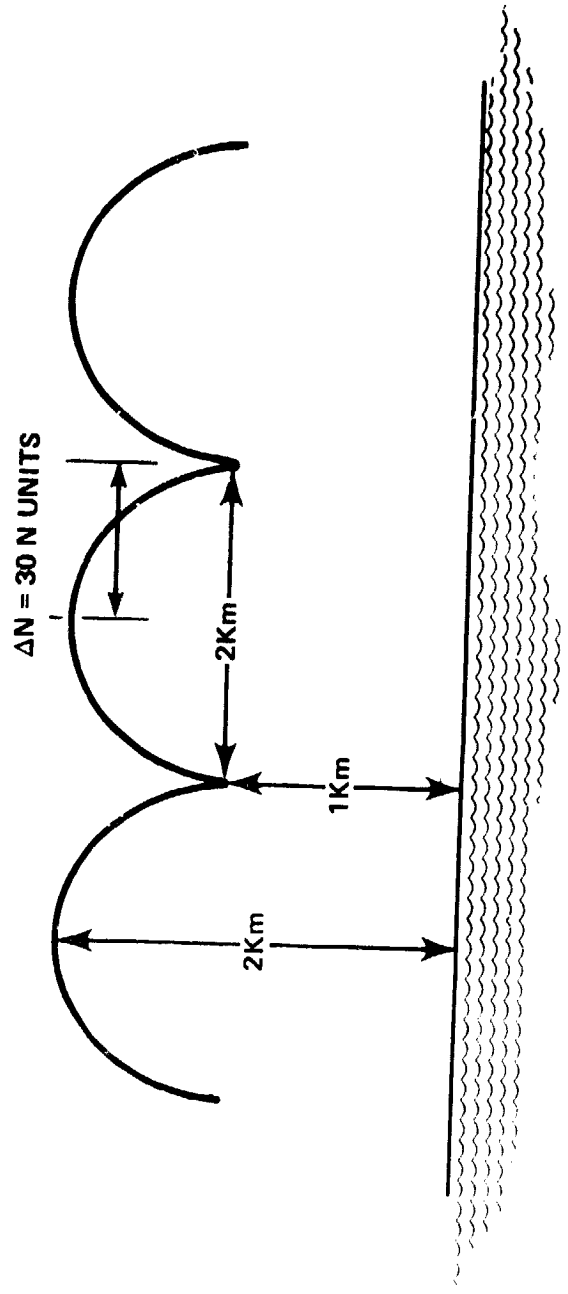

Fig. 18 Nominal Model of Convective Field at Wallops Island, Virginia

TABLE 5

SUMMARY OF NOMINAL SCALE DIMENSIONS FOR THE TROPOSPHERE

CUMULUS CLOUD

1) MEAN DIAMETERS (LOPEZ; 1977)

0.1 TO 6 KM

2) CLOUD STREETS (KUETTNER; 1971)

LENGTH 20 TO 500 KM

SPACING 2 TO 8 KM

SPACING-TO-HEIGHT RATIO 2 TO 4

CLEAR AIR CONVECTION

1) CELL DIAMETERS
2) CELL FIELDS

} APPROXIMATELY SAME AS CUMULUS

4.0 Range Errors Introduced by the Ionosphere

4.1 Range Error Correction

The excess group delay over a nadir propagation path, H, through the ionosphere relative to that same free space path is,

$$\Delta T = \frac{1}{c}\int_{o}^{H}(n-1)\ ds = \frac{1}{c}\int_{o}^{H}\Delta n\ ds \qquad (4.1)$$

where c = velocity of light

n = group refractive index

For propagation at frequencies considered here greater than 1 GHz), Δn is given by [Lawrence et al., 1964],

$$\Delta n \approx 40.3\ \frac{N}{f^2} \qquad (4.2)$$

where, N = electron density (electrons/m^3)

f = frequency in Hertz

Combining (4.2) and (4.1), the excess time delay introduced by the ionosphere over a range, R, is

$$\Delta T = 1.34 \times 10^{-7}\ \frac{N_T}{f^2} \qquad \text{[sec]} \qquad (4.3)$$

where N_T is the ionospheric electron content defined by,

$$N_T = \int_0^H N \, ds \qquad \left[\frac{\#}{m^2}\right] \tag{4.4}$$

The excess range correction introduced by the ionosphere, ΔH_i, is,

$$\Delta H_i = c \, \Delta T = 40.3 \, \frac{N_T}{f^2} \qquad [m] \tag{4.5}$$

In Fig. 19, we plot the correction, ΔH_i as a function of values of N_t ranging from those nominal (daytime) values at the minimum of the solar cycle ($N_t \approx 20 \times 10^{16}$ m^{-2}) to near the maximum ($N_t \approx 100 \times 10^{16}$ m^{-2}) for the frequencies of 6, 13.5 and 35 GHz. We note at the indicated minimum solar cycle, the respective range errors are 22.2, 4.4, and 0.7 cm and at the maximum solar cycle they are 112, 22.1, and 3.3 cm. These values establish nominal range corrections to be accounted for in any altimeter system.

4.2 Ionospheric Scale Size

Utilizing combinations of geostationary and orbiting satellite data, real time contours of electron content maps have been constructed by Davies [1978] and Davies et al [1977] (for near solar minimum), an example of which is depicted in Fig. 20. The indicated numbers when multiplied by 10^{15} represent the electron content values. We note that at latitudes between 20° and 30° and during mid- and late afternoon hours, relatively high gradients in the electron content may result. These translate to values as high as 2 cm/100 km at 13.5 GHz for the example cited.

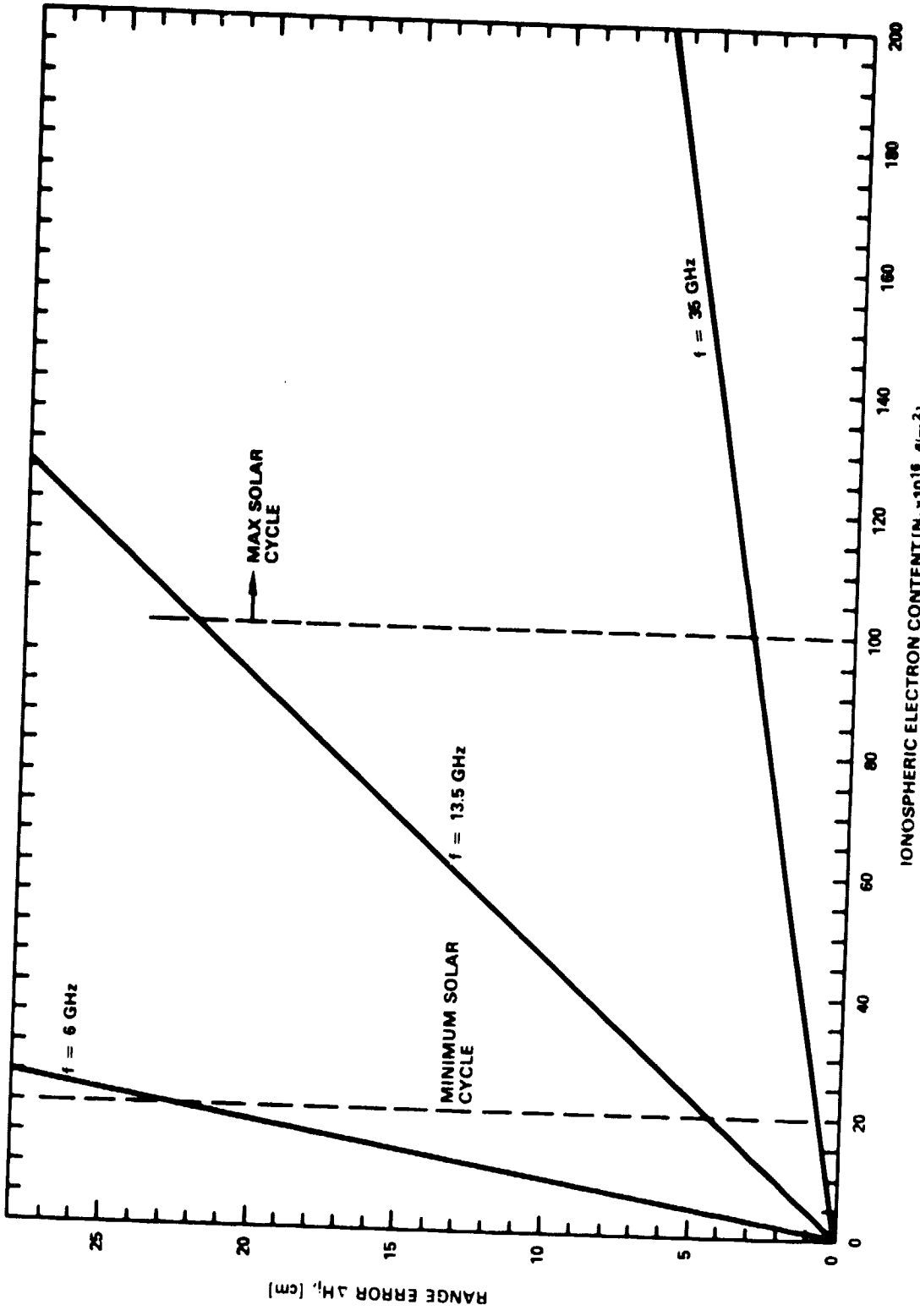

Fig. 19 Range Error as a Function of Ionosphere Electron Content at f = 6, 13.5 and 35 GHz

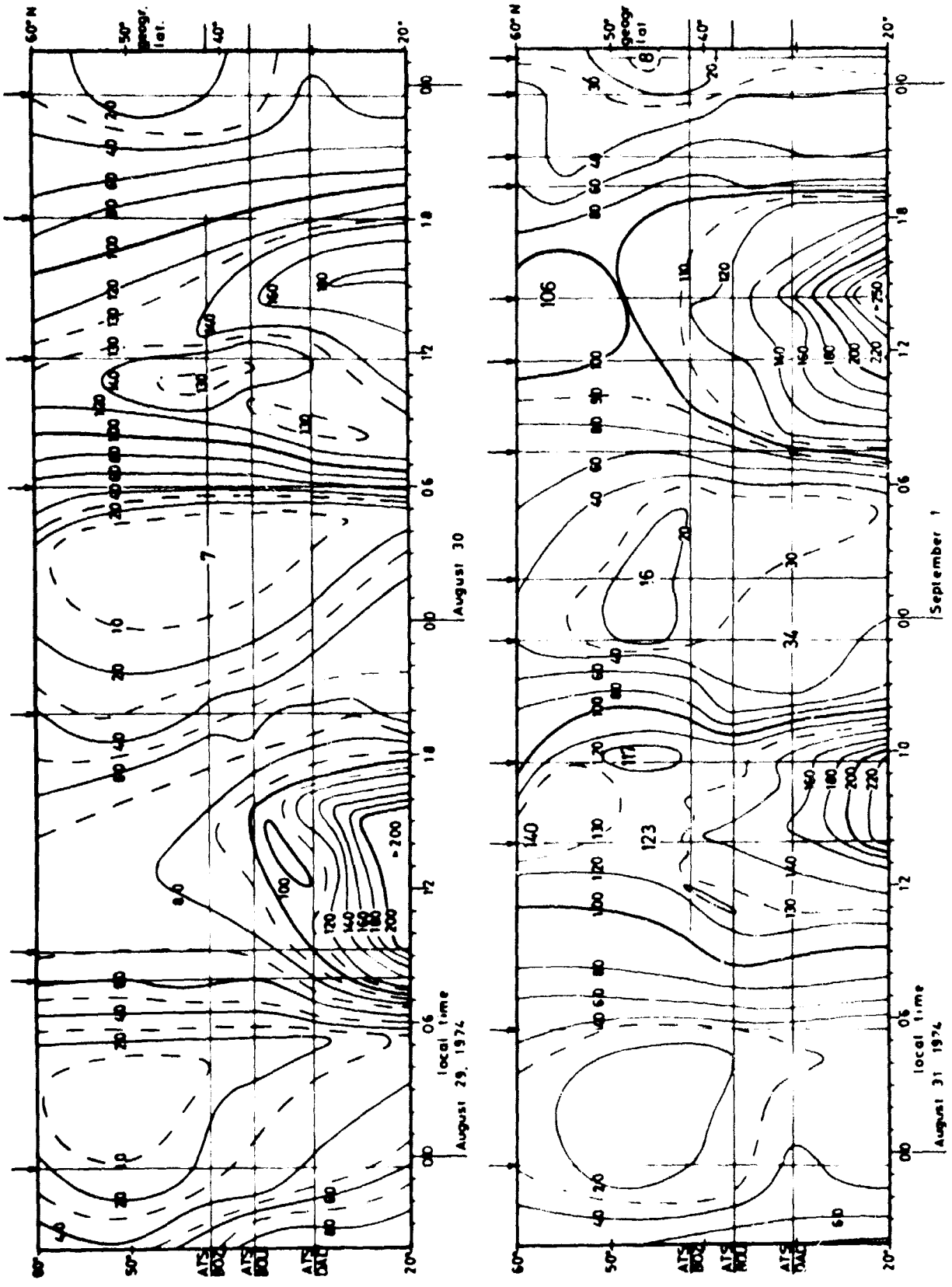

Fig. 20 Example of Contour Map of Total Electron Content, N_t, During Solar Minimum. Values indicated x10^{15}=N_t (Davies; 1978)

In addition to scale changes due to diurnal variations, ionospheric disturbances may result in as much as a 20% variation of the TEC over a 100 km distance in the mid-latitudes ($\pm$ 20°)*. During a solar maximum this gradient could translate into 4 cm/100 km for an electron content of 100 x 10^{16} electrons/m^2 at 13.5 GHz.

4.3 Faraday Rotation Technique

A technique employed for the Seasat A altimeter experiment to account for ionospheric group delay was to measure N_T using the Faraday Rotation Technique. The amount of Faraday Rotation, over a nadir range, H, is given by [Burns and Fremouw, 1970],

$$\Omega = 2.36 \times 10^{-5} \int_0^H B \cos\theta \; N \; ds \quad \text{[radians]} \qquad (4.6)$$

where θ is the angle between the wave normal and the earth's magnetic field (expressed above in gammas), N is the electron density in electrons/m^3, and H is in meters.

A disadvantage of the Faraday Rotation technique is the fact that the quantity

$$\int_0^H B \cos\theta \; N \; ds \qquad (4.7)$$

is measured rather than

*Private Communication on 4/18/80 with H. Soicher, U.S. Army Communications R and D Command, Ft. Monmouth, New Jersey. The above comment is based on Dr. Soicher's measurements of electron content.

$$\int_0^H N \, ds \qquad (4.8)$$

In arriving at (4.8), the term B cosθ in (4.7) is usually removed from the integral sign and replaced by its value at a "mean" ionospheric altitude (e.g., ~400 km (Klobuchar;1978)). Since B decreases inversely with the cube of the geocentric distance, and the electron density decreases exponentially with altitude above F_2 max (≈300 km), the integral is heavily weighted near the earth and is considered to provide electron content values for altitudes below ≈ 1200 km [Soicher 1975].

For the Seasat altimeter operation, Faraday rotation measurements were made at Goldstone, California and Armidale, Australia using the ATS-1 and ATS-2 geosynchronous satellite beacons. Total electron content measurements, N_T, were deduced at these stations and extrapolated to sub-satellite points on earth from an algorithm [Seasat User's Handbook, 1979; Wu, 1977] having the functional dependence given by,

$$N_T = f \{N_T(\text{min}), N_T(\text{max}), \chi, \phi_m, t\} \qquad (4.9)$$

where N_T(min), N_T(max) = minimum and maximum electron contents as measured at the stations

ϕ_m = geomagnetic latitude

χ = sun angle

t = local time

The accuracy of N_T prediction by extrapolating Faraday measurements at a single location to arbitrary sub-satellite points may be as high as 50% [Klobuchar; 1978], the actual level of uncertainty depends upon the year within the solar cycle, location, season, as well as the time of day. It may be noted that the most recent solar minimum occurred around 1974 [Oh;1974]. The standard deviation of values of electron content at any one location based on daily measurements over any one month was found to be nominally, 25% [Klobuchar,1978].

In an accuracy comparison between the Seasat algorithm and the model used by the Naval Service Weapon Center (NSWC), differences as much as 5 cm were noted for a Seasat pass on 9/13/78 [Tapley et al; 1979]. The latter model used daily measurements of the sunspot number (as measured at Boulder, Colorado) to obtain the electron content.

4.4 Two Altimeter Method Correction

A method by which continuous sub-orbital point ionospheric corrections may be obtained is described here. This method employs two altimeter systems at frequencies f_L and f_U (e.g., f_L = 6 GHz and f_U = 13.5 GHz; L and U denoting lower and upper frequencies). In Fig. 21 we depict the corresponding idealized transmitted pulses and the respective mean return wave forms at frequencies f_L and f_U. The times Δt_L and Δt_U represent the respective delays between the leading edge points of the transmitted pulses and the indicated leading edges of the mean return waveforms [Townsend, 1980].

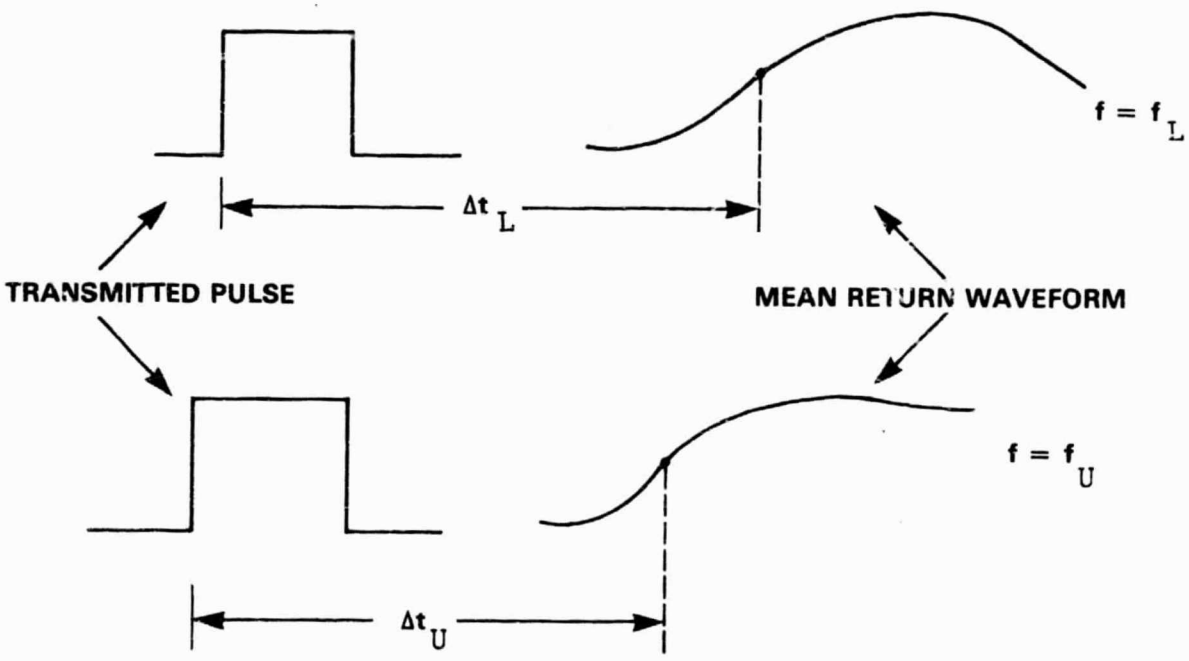

Fig. 21 Two Frequency Altimeter Method for Ionospheric Height Correction. Subscripts L and U denote Lower and Upper Frequencies, respectively.

These delays are related to the true range, H_T, in the following manner.

$$H_T = H_U - \Delta H_{iU} \tag{4.10}$$

$$H_T = H_L - \Delta H_{iL} \tag{4.11}$$

where H_U and H_L are the apparent measured ranges at f_U and f_L given by,

$$H_U = \frac{(c\ \Delta t_U)}{2} \tag{4.12}$$

$$H_L = \frac{(c\ \Delta t_L)}{2}$$

and ΔH_{iL} and ΔH_{iU} are the ionospheric height corrections given by (4.5) at f_L and f_U, respectively. We note that,

$$\left(\frac{\Delta H_{iL}}{\Delta H_{iU}}\right) = \left(\frac{f_U}{f_L}\right)^2 \equiv K \tag{4.13}$$

Injecting (4.13) into (4.10) and (4.11), and eliminating ΔH_{iU} and ΔH_{iL}, we obtain

$$H_T = \left(\frac{K}{K-1}\right) H_U - \left(\frac{1}{K-1}\right) H_L \tag{4.14}$$

Allowing σ_U and σ_L to represent the system standard deviations associated with the H_U and H_L measurements, respectively, it may be demonstrated that in subtracting out the ionospheric contributions and arriving at (4.14), the resultant uncertainty in H_T becomes,

$$\sigma_i = M \ \sigma_U \tag{4.15}$$

where,

$$M = \frac{1}{K-1} \left[K^2 + \left(\frac{\sigma_L}{\sigma_U} \right)^2 \right]^{\frac{1}{2}} \tag{4.16}$$

In (4.15) and (4.16), M denotes a multiplication factor introduced by the additional lower frequency altimeter system. We note that as the frequency separation increases, K assumes large values and $M \longrightarrow 1$. In Fig. 22 are plotted values of M as a function f_L where it is assumed that f_U = 13.5 GHz. The different curves correspond to various assumed uncertainty levels in the measurement of H_L. We note that at f_L = 6 GHz and $\sigma_L = \sigma_U$ = 2 cm (Seasat case for σ_U),

$$\sigma_i = 2.5 \text{ cm} \tag{4.17}$$

The two frequency altimeter system thus eliminates the range uncertainty due to the ionosphere although an increase of error of 0.5 cm (e.g., from 2 to 2.5 cm) does occur as compared

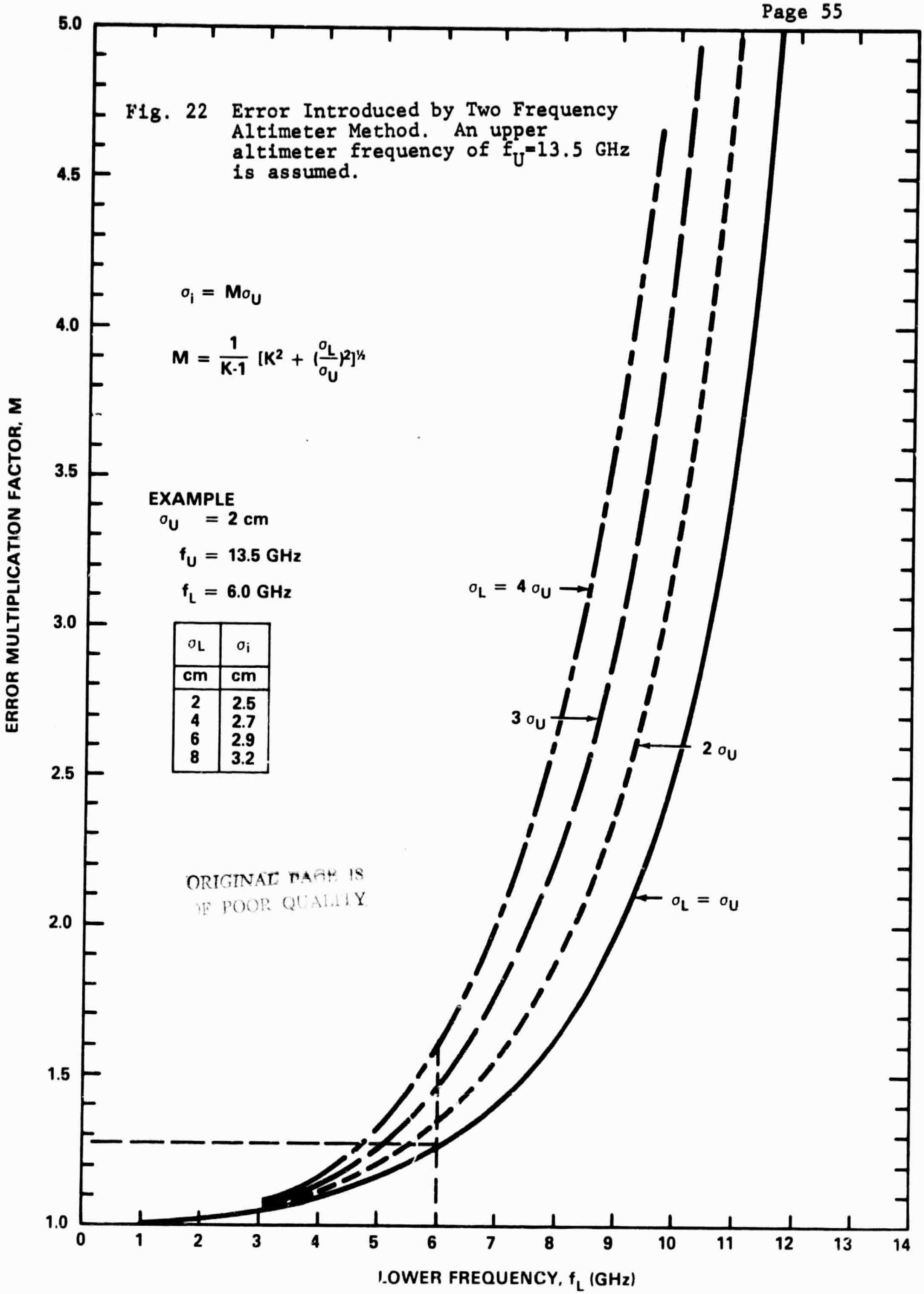

Fig. 22 Error Introduced by Two Frequency Altimeter Method. An upper altimeter frequency of f_U=13.5 GHz is assumed.

σ_L	σ_i
cm	cm
2	2.5
4	2.7
6	2.9
8	3.2

to that of the single frequency case (for the example considered).

An important byproduct of the two altimeter system is that it would provide highly accurate measurements of continuous swaths of the ionospheric electron content. Such measurements would be capable of "filling in" large gaps in regions over the oceans where few measurements exist and hence, establish measured worldwide scale size information. It would thus provide to the engineer information on range error variability necessary for the design of future high precision altimeter missions.

5.0 Summary and Conclusion

In Table 6, we summarize the nominal uncorrected atmospheric height errors for the troposphere and ionosphere in the absence of rain effects. We note the dry tropospheric term due to all the atmospheric constituents with the exception of water vapor, is significantly larger than the wet term, due only to water vapor. However, the variability of the dry term is significantly less than that of the wet term and the uncertainty in predictability is significantly smaller. The ionospheric correction depends on the time of day, location, season, and year with the solar cycle. Nominal day time mid-latitude values are shown at the three frequencies where "MIN" and "MAX" denote electron contents of $N_T = 20 \times 10^{16}$ electrons/m^2 (solar min) and 100×10^{16} electrons/m^2 (solar max).

In Table 7, we summarize the height uncertainties (rms) after the implementation of atmospheric corrections assuming the indicated modes of operation as described by column (1). For example, Row A denotes a satellite containing a two frequency altimeter (13.5 and 6.0 GHz), and a radiometer system. Column (2) indicates "rain" or "no rain", the former case generally disallowing radiometer measurements of the wet term. Column (3) corresponds to uncertainties in removing the range errors for the wet term in the troposphere when a radiometer is used, and columns (4) and (5) apply when theoretical models are incorporated. Column (6) gives the additional uncertainty in the removal of the ionospheric correction when a two frequency altimeter is employed

Table 6

SUMMARY OF NOMINAL ATMOSPHERIC UNCORRECTED HEIGHT ERRORS FOR THE TROPOSPHERE AND IONOSPHERE

TROPOSPHERE (CM)		IONOSPHERE (CM)					
		f = 13.5 GHz		f = 6 GHz		f = 35 GHz	
DRY	WET	MIN	MAX	MIN	MAX	MIN	MAX
230-234	5-35	4	22	22	113	0.5	3

Table 7

NOMINAL HEIGHT UNCERTAINTIES AFTER ATMOSPHERIC CORRECTIONS ARE IMPLEMENTED

Row	MODE	WEATHER CONDITION	TROPOSPHERE (CM)			IONOSPHERE (CM)		TOTAL UNCERT.
			RADIOM.	MODEL - FNWC		TWO FREQ. ALTIM.	FARAD. ROTAT.	
			WET	WET	DRY			CM
	(1)	(2)	(3)	(4)	(5)	(6)	(7)	(8)
A	1. 2 Freq. Altim. 2. 2 Freq. Radiom. 3. Dry Term Model	NO RAIN	2.5		2	0.5		3
B	1. 2 Freq. Altim. 2. Wet Term Model 3. Dry Term Model	RAIN		6	2	0.5		6.5
C	(Seasat Case) 1. SMMR 2. Ionos. Model 3. Dry Term Model	NO RAIN	2.5		2		5	6
D	(Seasat Case) 1. Wet Term Model 2. Dry Term Model 3. Ionos. Model	RAIN		6	2		5	8

and (7) when employing the Seasat ionospheric algorithm. Column (8) represents the total uncertainty (square root of the sum of squares of individual errors).

In comparing the various total uncertainties in Table 7 (rows A and C), we note that the employment of a two frequency altimeter system results in an nominal net atmospheric precision of 3 cm as compared to 6 cm assuming the Seasat system. Since the ionospheric correction is continuously and systematically implemented along track with the two frequency method, significantly larger peak uncertainties (e.g., 5 cm) are expected to be removed. A byproduct result of such a system would be to provide (for the first time) a world wide continuous swath of the electron content (integrated columnar electron density). Aside from providing pertinent data to ionospheric physicists, such data would be extremely useful in establishing scale variabilities of ionospheric electron content; a useful input in the design of future altimeter missions.

The feasibility of gating rain reflectivity with the altimeter system is established in Chapter 2. Such a capability would provide the experimenter with an accurate estimate of rain rates (mm/hr) at various altitudes. Such results could be employed in culling of the data, providing ancillary information to the altimeter measurements. A continuous track of rain rates values could also provide the meteorologist with quantitative information on a world wide scale over the oceans where relative little rain measurements exist.

In incorporating a radiometer system for removing the wet contribution, the radiometer antenna beams should generally be coincident with that of the altimeter system. This would tend to insure that the height corrections apply to the same column of the troposphere unlike the SMMR on Seasat. (The SMMR had variable footprints of 21 km at 37 GHz to 121 km at 6.6 GHz and the main beam was offset from nadir by approximately 50^{o} [Dunne, 1978].)

Also suggested in a future high precision altimeter mission is a nadir pointing coincident infrared radiometer for the detection of clouds (e.g., at 10 microns). This device would prove highly useful in establishing correlation between possible anomalous height variations and the presence of cloud [Grody, 1976].

6.0 References

Bean, B.R. and E. J. Dutton, [1978], "Radio Meteorology", Dover Publications, New York.

Burns, A.A. and E.J. Fremouw, [1970], "A Real Time Correction Technique for Trans-ionospheric Ranging Error", IEEE Trans. on Anten. and Prop., Vol. AP-18, No. 6, November, pp. 785-790.

Campen, C.F.,Jr., R.M. Cunningham, V.G. Plank [1961], "Electromagnetic Wave Propagation in the Lower Atmosphere", Chapter 13 of Handbook of Geophysics, MacMillan Co., New York, pp. 13-5 to 13-11.

C.C.I.R. International Radio Consultative Committee, [1978], Recommendations and Reports of the C.C.I.R., XIVth Plenary Assembly, Kyoto, Vol. V, Propagation in Non-Ionized Media.

C.C.I.R. Document 5/23-E, Canada, 22 October [1975], Study Program 5C-2/5, "Propagation Data Required for Space Telecommunication Systems".

Cole, A.E., A. Court and A.J. Kantor, [1965], "Model Atmospheres" in Handbook of Geophysics and Space Environments, edited by S.L. Valley, pp. 2-11 - 2-13, McGraw-Hill, New York.

Cole, A.E. and A.J. Kantor [1963], Air Force Interim Supplemental "Atmospheres to 90 Kilometers", AF Surv. Geophys., No. 153, Air Force Cambridge Research Laboratories, Hanscom AFB, Mass.

Cunningham, R.M. [1964], "Meteorological Aspects of Range and Range Rate Error", AFCRL Report ESD-TO-4-64-103.

Davies, K. [1978], "Forecasting and Prediction of Ionospheric Parameters", AGARD Lecture Series No. 93, Recent Advances in Radio and Optical Propagation for Modern Communications, Navigation and Detection Systems, pp. 6-1 to 6-29.

Davies, K., G.K. Hartmann and R. Leitinger [1977], "A Comparison of Several Methods of Estimating the Columnar Electron Content of the Plasmasphere", J. Atmos. Terr. Res., Vol. 39, pp. 571-580.

References (Contd.)

Doviak, R.J. and D. Zrnic [1979], "Receiver Bandwidth Effect on Reflectivity and Doppler Velocity Estimates", J. Appl. Meteorol., Vol. 18, No. 1. pp. 70-76, January.

Dunne, J.A., [1978], "The Experimental Oceanographic Satellite Seasat-A", Boundary-Layer Meteorology, Vol. 13, pp. 393-404.

Edgar, A.K., E.J. Dodsworth and M.P. Warden [1973], "The Design of a Modern Surveillance Radar", International Conference on Radar - Present and Future, 23-25 October, IEE Conference Publication No. 105, pp. 8-13.

Essen, L. and K.D. Froome [1951], "The Refractive Indices and Dielectric Constants of Air and Its Principal Constituents at 24000 Mc/s", Prec. Phys. Soc. (London, England), Vol. 64, October, pp. 862-875.

Goldhirsh, J., [1979], "A Review on the Application of the Non-Attenuating Frequency Radars for Estimating Rain Attenuation and Space Diversity Performance", IEEE Trans. on Geoscience Electronics, Vol. GE-17, No. 4, October, pp. 218-239.

Goldhirsh, J. and I. Katz, [1979], "Useful Experimental Results for Earth-Satellite Rain Attenuation Modeling", IEEE Trans. on Anten. and Prop., Vol. AP-27, pp. 413-415.

Goldhirsh, J., [1977], "Analysis of Single and Multiple Wavelength Radar Systems for Estimating Slant Path Attenuation Through Rain and Cloud at Frequencies Greater than 10 GHz", APL/JHU Technical Report S1R77U-036, October.

Grody, N.C., [1976], "Remote Sensing of Atmospheric Water Content from Satellites Using Microwave Radiometry", Trans. on Anten. and Prop., Vol. AP-24, No. 2, March, pp. 155-162.

Gunn, K.L.S. and T.W.R. East [1954], "The Microwave Properties of Precipitation Particles", Quart. J. Roy. Meteorol. Soc., Vol. 80, pp. 522-545.

References (Contd.)

Gunn, K.L.S. and G.D. Kinzer, [1949], "The Terminal Velocity of Fall of Water Droplets in Stagnant Air", J. Meteorology, Vol. 6, pp. 243-248.

Klobuchar, J.A., [1978], "Ionospheric Effects on Satellite Navigation and Air Traffic Control Systems", AGARD Lecture Series No. 93, Recent Advances in Radio and Optical Propag. for Modern Communications, Navigation and Detection Systems, pp. 7-1 to 7-17.

Konrad, T.G., [1978], "Statistical Models of Summer Rainshowers Derived from Fine-Scale Radar Observations", J. Appl. Meteorol., Vol. 17, No. 2, pp. 172-188, February.

Konrad, T.G. and F.L. Robison, [1973], "Development and Characteristics of Free Convection in the Clear Air as Seen by Radar and Aircraft", J. of Appl. Meteorol., Vol. 12, No. 8, December, pp. 1284-1294.

Konrad, T.G., [1970a], "The Dynamics of the Convective Process in the Clear Air as Seen by Radar", 14th Radar Meteorology Conference, November 17-20, Tucson, Arizona, American Meteorological Society, pp. 57-67.

Konrad, T.G., [1970b], "The Dynamics of the Convective Process in Clear Air as Seen by Radar", J. of Atmospheric Sciences, Vol. 27, No. 8, November, pp. 1138-1147.

Kuettner, J.P., [1971], "Cloud Bands in the Earth's Atmosphere - Observation and Theory", Tellus, Vol. 23, pp. 404-425.

Lawrence, R.S., C.G. Little and H.J.A. Chivers, [1964], "A Survery on Ionospheric Effects Upon Earth-Space Radio Propagation", Proc. IEEE, Vol. 52, pp. 4-27, January.

Laws, J.O. and D.A. Parsons, [1943], "The Relation of Raindrop Size to Intensity", Trans. Amer. Geophys. Union, Vol. 22, pp. 709-721.

Lipes, R.G., [1979], "Altimeter Path Correction", JPL IOM 331-78-166A - Jet Propulsion Laboratory, Calif. Institute of Technology, Pasadena, California.

References (Contd.)

Lorell, J., [1979], "Altimeter Signal Anomalies Due to Sea-Surface, Waveheight and Tracking System Effects", Seasat Colloquim, October 29 - November 1, Scripps Institution of Oceanography, La Jolla, California.

Lopez, R.E., [1977], "The Lognormal Distribution and Cumulus Cloud Populations", Monthly Weather Review, Vol. 105, July, pp. 865-872.

Nagler, R.G. and D.N. Brown, [1979], "Ocean Current Monitoring from Space", System Planning Corporation, SPC Log No. 80-0148 (1500 Wilson Boulevard, Suite 1500, Arlington, Virginia 22209).

Nathanson, F.E. and P.L. Smith, Jr., [1972], "A Modified Coefficient for the Weather Radar Equation", in Proc. 15th Radar Meteorol. Conf., Urbana-Champaign, IL, American Meteorological Society, pp. 228-230, October 10-12.

Nathanson, F.E., [1969], "Radar Design Principles", McGraw Hill Book Co., pp. 206-209.

Oguchi, T., [1973], "Attenuation and Phase Rotation of Radio Waves Due to Rain Calculations at 19.3 and 34.8 GHz", Radio Science, Vol. 8, No. 1, January, pp. 31-38.

Oh, In Hwan, [1974], "The Average Solar Flux (10.7 cm) Model For an 11-Year Cycle", Wolf Research and Development Corporation, NAS 5-11933 MOD. 13, September.

Olsen, R.L., D.V. Rogers and D.B.Hodge, [1978], "The aR^b Relation in the Calculation of Rain Attenuation", IEEE Trans. Anten. and Prop., Vol. AP-26, No. 2, March, pp. 318-329.

Ray, P.S., [1972], "Broadband Complex Refractive Indices of Ice and Water", Appl. Opt., Vol. II, pp. 1836-1844.

Rogers, D.V. and R.L. Olsen, [1975], "Delay and Its Relation to Attenuation in Microwave Propagation Through Rain", USNC/URSI Annual Meeting, Boulder, Colorado, October 20-23.

References (Contd.)

Saastamoinem, J., [1972], "Atmospheric Correction for the Troposphere and Stratosphere in Radio Ranging of Satellites", Geophysical Mongraph # 15, American Geophysical Union, Washington, D.C., William Byrd Press, Richmond, Va.

Seasat (Gulf of Alaska) Workshop Report, [1979], Vol. 1, Panel Reports, National Aeronautics and Space Administration, (Published by Jet Propulsion Laboratory, California Institute of Technology, Pasadena, California, April) (G22-101).

Seasat (Interim Geophysical Data Record) User's Handbook - Initial Version - Altimeter, [1979], National Aeronautics and Space Administration, Published by Jet Propulsion Laboratory, California Institute of Technology, Pasadena, California 91103, April, (622-97).

Setzer, D.E., [1970], "Computed Transmission Through Rain at Microwave and Visible Frequencies", Bell System Technical Journal, Vol. 49, No. 8, October.

Skolnik, M.I., [1974], "The Application of Satellite Radar for the Detection of Precipitation", NRL Memorandum Report 2896, October (N.R.L., Washington, D.C.).

Smith, E.K. and S. Weintraub, [1953], "The Constants in the Equation for Atmospheric Refractive Index at Radio Frequencies", Proc. IRE, Vol. 41, August, pp. 1035-1037.

Soicher, H., [1977], "Ionospheric and Plasmaspheric Effects in Satellite Navigation Systems", IEEE Trans. on Anten. and Prop., Vol. AP-25, No. 5, September, pp. 705-708.

Soicher, H., [1975], "Plasmaspheric Contribution to Group-Path-Delay of Trans-ionospheric Satellite Navigation-Signals", AGARD Conference Proceedings No. 173, on Radio Systems and the Ionosphere, EM Wave Prop. Panel, Athens, Greece, 26-30 May, pp. 6-1 to 6-15.

References (Contd.)

Tapley, B.D., B.E. Schutz, J.G. March, W.F. Townsend, and G.H. Barn Editors [1979], "Accuracy Assessment of the Seasat Orbit and Height Measurement", Institute for Advanced Study in Orbital Mechanics (IASOM TR 79-5), The University of Texas at Austin, Austin, Texas, October.

Townsend, W.F., [1980], "On Initial Assessment of the Performance Achieved by the Seasat-1 Radar Altimeter", NASA Technical Memorandum 73279, NASA Wallops Flight Center, Wallops Island, Virginia 23337.

Van De Hulst, H.C., [1957], "Light Scattering by Small Particles", New York; John Wiley Sons, Inc., 1957.

Wu, S.C., [1977], "Ionospheric Calibration for Seasat Altimeter", JPL Engineering Memorandum 315-34, Jet Propulsion Laboratory, California Institute of Technology, Pasadena, California.